Late Holocene climate: Natural or anthropogenic?

W. F. Ruddiman[1], D. Q. Fuller[2], J. E. Kutzbach[3], P. C. Tzedakis[4], J. O. Kaplan[5], E. C. Ellis[6], S. J. Vavrus[3], C. N. Roberts[7], R. Fyfe[7], F. He[3,8], C. Lemmen[9], and J. Woodbridge[7]

[1]Department of Environmental Sciences, University of Virginia, Charlottesville, Virginia, USA, [2]Institute of Archaeology, University College London, London, UK, [3]Center for Climatic Research, University of Wisconsin-Madison, Madison, Wisconsin, USA, [4]Environmental Change Research Centre, Department of Geography, University College London, London, UK, [5]ARVE Group, Environmental Engineering Institute, Ecole Polytechnique Federale de Lausanne, Lausanne, Switzerland, [6]Department of Geography and Environmental Systems, University of Maryland, Baltimore County, Catonsville, Maryland, USA, [7]School of Geography, Earth and Environmental Sciences, University of Plymouth, Plymouth, UK, [8]College of Earth, Ocean, and Atmospheric Sciences, Oregon State University, Corvallis, Oregon, USA, [9]Center for Materials and Coastal Research, Helmholtz-Zentrum Geesthacht, Geestracht, Germany

Abstract For more than a decade, scientists have argued about the warmth of the current interglaciation. Was the warmth of the preindustrial late Holocene natural in origin, the result of orbital changes that had not yet driven the system into a new glacial state? Or was it in considerable degree the result of humans intervening in the climate system through greenhouse gas emissions from early agriculture? Here we summarize new evidence that moves this debate forward by testing both hypotheses. By comparing late Holocene responses to those that occurred during previous interglaciations (in section 2), we assess whether the late Holocene responses look different (and thus anthropogenic) or similar (and thus natural). This comparison reveals anomalous (anthropogenic) signals. In section 3, we review paleoecological and archaeological syntheses that provide ground truth evidence on early anthropogenic releases of greenhouse gases. The available data document large early anthropogenic emissions consistent with the anthropogenic ice core anomalies, but more information is needed to constrain their size. A final section compares natural and anthropogenic interpretations of the $\delta^{13}C$ trend in ice core CO_2.

1. Introduction

During the 1900s, paleoclimate scientists assumed that the warmth of the last 10,000 years was caused by natural changes in Earth's orbit. Previous orbital alignments had melted the Northern Hemisphere ice sheets and propelled climate into a warm interglacial state [*Imbrie et al.*, 1992; *Bradley*, 1999]. Observed climate then remained nearly stable during the Holocene (Figure 1), except for cooling at high northern latitudes. Implicit in this view was a return of glacial climate sometime in the future as a continuation of the 2.75 million year history of natural glacial-interglacial cycles [*Hays et al.*, 1976; *Shackleton et al.*, 1984; *Raymo et al.*, 1989].

Consistent with this view, two hypotheses have called on processes internal to the climate system to account for the 20 ppm CO_2 (carbon dioxide) increase during the last 7000 years that has helped keep climate warm. The carbonate compensation hypothesis [*Broecker et al.*, 1999] viewed the CO_2 increase as a delayed recovery from an earlier imbalance in ocean chemistry initiated by extraction of ocean carbon and sequestration in northern forests late in the last deglaciation. The coral reef hypothesis [*Ridgwell et al.*, 2003] interpreted the CO_2 trend as resulting from deposition of $CaCO_3$ in coral reefs as sea level stabilized, with an accompanying release of CO_2 from the ocean to the atmosphere.

In 2003, two lines of evidence formed the basis for a challenge to the natural view [*Ruddiman*, 2003]. First, the atmospheric CO_2 and CH_4 (methane) increases of the last few millennia were found to be anomalous compared to decreases during the preceding interglaciations. Second, agriculture spread across the continents during those same millennia and emitted anthropogenic greenhouse gases that overprinted natural trends. Clearing of forests for crops and pastures required cutting forests and emitted CO_2, while flooding of rice paddies, domesticating livestock, and burning crop residues emitted CH_4. In this view, greenhouse gases from preindustrial farming were large enough to warm climate and prolong the natural interglacial warmth initiated by orbital variations (Figure 1).

Here we summarize new evidence that moves this debate forward by evaluating a wide range of evidence to test the predictions of the natural and anthropogenic hypotheses. The first ("top-down") evaluation compares
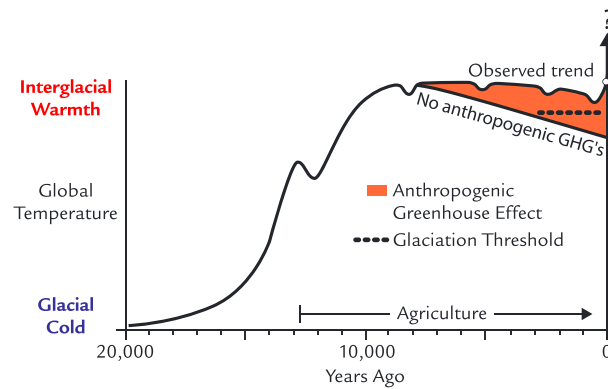
Figure 1. Schematic summary of two views of Holocene climate. Natural hypotheses regard the nearly stable observed climate trend as natural in origin, but the anthropogenic hypothesis claims that climate would have naturally cooled and passed the threshold for early glacial inception if anthropogenic greenhouse gas emissions had not offset most of a natural cooling.

Holocene trends of the greenhouse gases CO_2 and CH_4 and two independent indices of regional temperature responses (Antarctic δD and deep-sea $\delta^{18}O$) to those during previous interglaciations. Natural explanations of the Holocene trends predict responses similar to those in the earlier interglaciations; the anthropogenic explanation predicts different responses. This top-down evaluation also updates the search for the closest Holocene insolation analog among previous interglaciations. The second ("bottom-up") evaluation explores paleoecological and archaeological syntheses that provide ground truth evidence about early anthropogenic releases of greenhouse gases. A final section compares natural and anthropogenic interpretations of the $\delta^{13}C$ trend in ice core CO_2.

2. Top-Down Evidence

The first evaluation of the two hypotheses focuses on an ice core sequence recovered by drilling at Dome C Antarctica [*European Project for Ice Coring in Antarctica (EPICA) Community Members*, 2004] which spans the last 800,000 years and records climatically diagnostic changes in atmospheric CO_2 and CH_4 concentrations and the deuterium/hydrogen (δD) ratio during previous interglaciations. Benthic $\delta^{18}O$ trends in marine sediments also span this interval [*Lisiecki and Raymo*, 2005]. Because pre-Holocene climates were not influenced by preagricultural people, these signals during previous interglaciations document the natural operation of the climate system prior to human intervention [*Ruddiman*, 2003]. Comparing them to the Holocene trends provides a way to assess the natural and anthropogenic explanations.

2.1. Comparison to Previous Interglaciations

In the discussion that follows, all interglaciations are aligned on the first interglacial $e\sin\omega$ maximum (e is eccentricity and $\sin\omega$ is the phase of Earth's precessional motion). $E\sin\omega$ maxima mark Northern Hemisphere summer insolation minima at the orbital precession cycle. For the current interglaciation, this level occurred about 900 years ago. Interglaciations are commonly referred to by marine isotopic stage (MIS) designations, with substages designated by letters. In this paper, the use of the term "stage" refers to the earliest part of each interglaciation immediately following the prior deglaciation.

The early anthropogenic hypothesis [*Ruddiman*, 2003] originated from the observation that late Holocene CO_2 and CH_4 trends differed from those during comparable intervals of interglacial stages 5, 7, and 9 in Vostok Station ice based on the GT4 gas age model [*Petit et al.*, 1999]. Similar evidence for anomalous Holocene behavior is apparent in gas trends at Dome C Antarctica based on the EDC3 gas age model [*Parrenin et al.*, 2007]. The increases in CO_2 concentrations since 7000 years ago and CH_4 concentrations since 5000 years ago differ from the prevalent downward trends during equivalent intervals in previous interglaciations (Figures 2a and 2b), except for the intermediate CO_2 trend during stage 15, which will be discussed later.

The CO_2 and CH_4 trends at Dome C vary widely among previous interglaciations [*Ruddiman et al.*, 2011] because of differences in timing and amplitude of the orbital elements obliquity (ε) and eccentricity-modulated precession ($e\sin\omega$) [*Milankovitch*, 1941; *Berger*, 1978]. To address the problem posed by variable interglacial trends, stacked-average trends for CO_2 and CH_4 are compiled in 1000 year bins (Figures 3a and 3b). The rising Holocene CO_2 and CH_4 concentrations after 7000 and 5000 years ago differ from the continuing downward trends during previous interglaciations. These anomalous CO_2 and CH_4 trends disagree with the natural hypotheses but are consistent with a large early anthropogenic overprint.
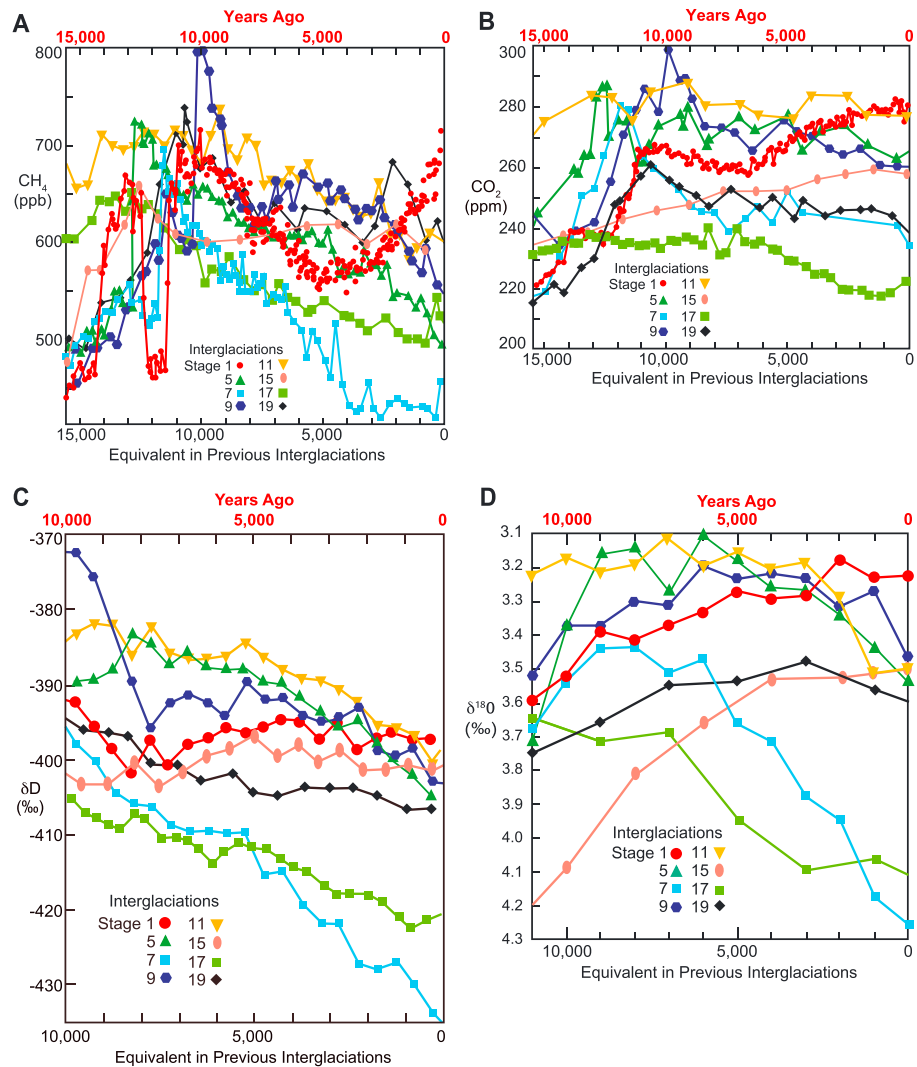
Figure 2. Holocene climate-related indices (in red) compared to previous interglaciations. (a, b) CH_4 and CO_2 signals from Dome C Antarctica [*Monnin et al.*, 2001; *EPICA Community Members*, 2004] based on EDC3 gas-phase age model [*Parrenin et al.*, 2007], (c) δD trends from Dome C [*EPICA Community Members*, 2004] based on EDC3 solid-phase age model [*Parrenin et al.*, 2007], and (d) $\delta^{18}O$ signals from the marine benthic stack using marine age model [*Lisiecki and Raymo*, 2005].

The δD (deuterium/hydrogen) ratio primarily records surface temperature over Antarctica [*Jouzel et al.*, 2003]. Holocene δD changes are variable along the lower ice sheet margins but relatively coherent and stable among high-altitude sites in East Antarctica, including Dome C [*Masson et al.*, 2000]. The EDC3 age model for δD variations at Dome C [*Parrenin et al.*, 2007] is based on the solid (ice) phase. At Dome C, the Holocene δD trend stays level for the last 6000 years, but the trends in previous interglaciations move toward more negative (colder) values during the equivalent intervals, except for stage 15, which again follows an intermediate trend (Figure 2c). The contrast between the stable late Holocene δD signal at Dome C and the negative trend in the previous interglacial average (Figure 3c) is again consistent with an anomalous (anthropogenic) origin but not a natural one.

Measurements of $\delta^{18}O$ in benthic foraminifera record some combination of changing global ice volume and deep-ocean temperature. A benthic $\delta^{18}O$ synthesis from dozens of cores from the major ocean basins [*Lisiecki and Raymo*, 2005] is widely used to represent this response. The age model for this signal follows the tuning philosophy of the Spectral Mapping Project group [*Imbrie et al.*, 1984] by assigning a lag of the filtered 41,000 year $\delta^{18}O$ signal behind the astronomically calculated summer insolation forcing at the 41,000 year obliquity period. The age model for the Holocene $\delta^{18}O$ signal is based on Th/U-adjusted ^{14}C measurements.
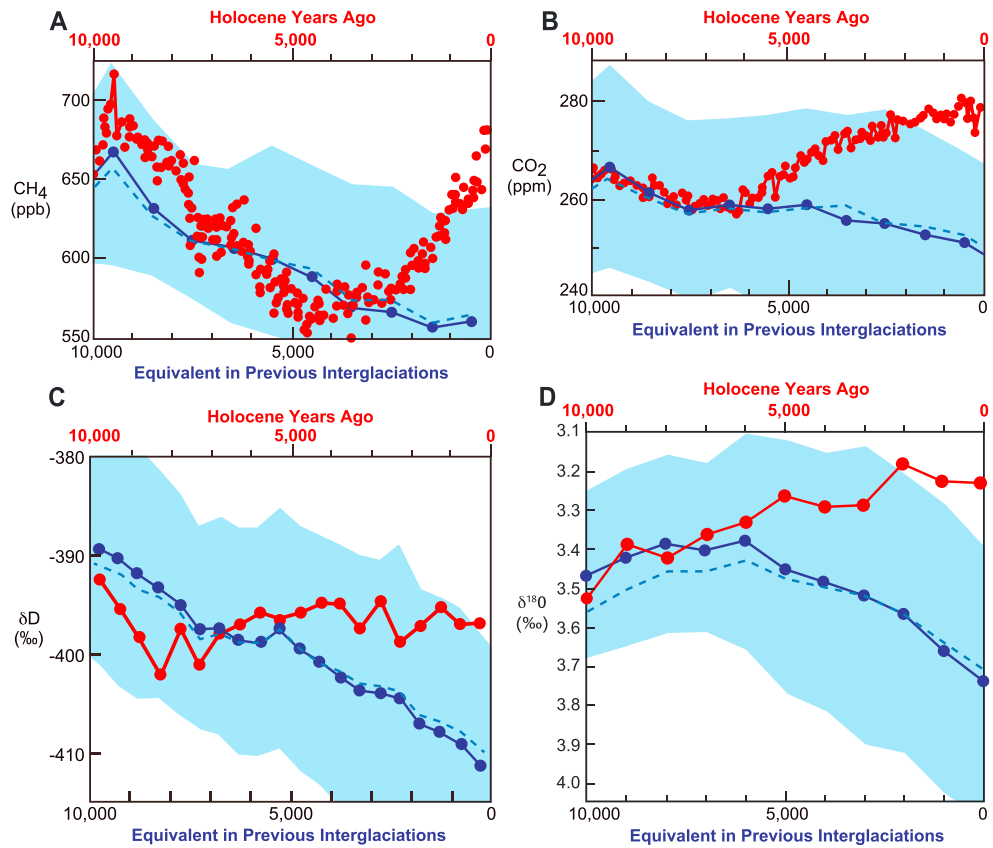
Figure 3. Comparison of Holocene trends (red) to stacked averages for previous interglaciations (blue). The light blue shading shows one standard deviation. (a) CH_4, (b) CO_2, (c) δD, and (d) $\delta^{18}O$ from sources listed in Figure 2 caption. Dome C CO_2 and CH_4 data for pre-Holocene interglaciations calculated by binning at 1000 year intervals. Dome C δD data calculated as binned 500 year averages for stages 1 to 11 and by interpolation between actual values for stages 15 to 19. $\delta^{18}O$ data for all interglaciations are binned averages from the benthic stack [*Lisiecki and Raymo*, 2005]. Stage 15 is excluded in the average shown by the solid blue line and included in the trend shown by the dashed line. Recent CO_2 reanalyses [*Bereiter et al.*, 2015] shift the previous interglacial average upward by ~1 ppm but retain the same downward trend.

Previous analyses showed a difference between the Holocene $\delta^{18}O$ response and those during interglacial stages 5, 7, and 9 [*Ruddiman*, 2007]. That assessment is updated in Figure 2d to include interglaciations prior to stage 9. The Holocene $\delta^{18}O$ signal remains at full interglacial values during the last 7000 years, whereas trends in most previous interglaciations (except stage 15) move toward more "glacial" conditions (colder deep-ocean temperatures and/or greater ice volume). As a result, the average $\delta^{18}O$ trend for the previous interglaciations differs from the Holocene signal (Figure 3d). A newer compilation for the Holocene shows no significant $\delta^{18}O$ change from 7000 years ago to the present [*Stern and Lisiecki*, 2015].

Along with the average trends of all four signals during previous interglaciations, Figure 3 shows a one standard deviation envelope. In each case, the Holocene signal moves outside this envelope during the last 1 or 2 millennia. Most of this envelope of variation is not caused by sample-to-sample noise within interglaciations, but by the widely varying ranges of the signal among the interglaciations, likely due to differences in orbital forcing.

As noted above, the trends in Figures 2 and 3 are aligned on the first $esin\omega$ maximum within each interglaciation. In contrast, two other methods aligned stage 1 with previous interglacial stage 11 using the start of the preceding deglaciations defined by δD trends [*EPICA Community Members*, 2004] and by CO_2 signals [*Broecker and Stocker*, 2006].

In contrast to these choices, the signal most commonly used to define past glacial-interglacial cycles is the benthic $\delta^{18}O$ record [*Lisiecki and Raymo*, 2005], which is used in Figure 4 to align all deglaciations. The deglaciation preceding the Holocene (as well as those prior to interglacial stages 5, 7, 9, and 19) lasted about
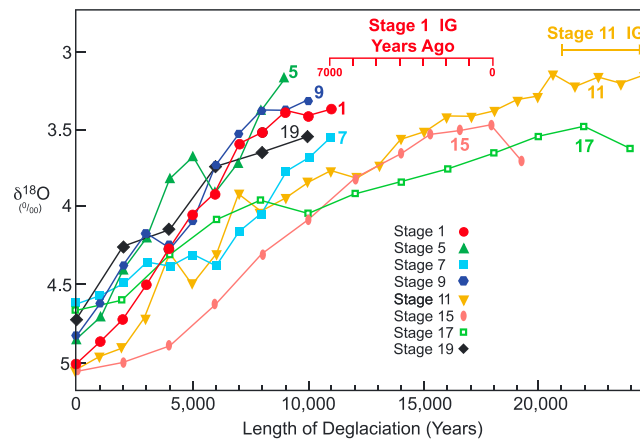
Figure 4. Varying lengths of deglaciations preceding full interglacial (IG) climates based on decreases in benthic foraminiferal $\delta^{18}O$ values [*Lisiecki and Raymo*, 2005]. The pre-Holocene deglaciation (and four others) lasted ~10,000 years, but the deglaciation preceding stage 11 lasted 20,000 years. Using this alignment method, stages 1 and 11 do not overlap.

10,000 years, while the one preceding stage 11 lasted more than 20,000 years. As a result of this large difference in lengths, the $\delta^{18}O$ deglacial alignment method places the entire stage 1 interglaciation within the late phase of the long deglaciation preceding stage 11, and the two full interglaciations do not even overlap. A similar misalignment would occur with attempts to align the Holocene interglaciation with stages 15 and 17 using this method. These misalignments disqualify stages 11, 15, and 17 for comparisons to the Holocene using this method, and the four remaining interglaciations (stages 5, 7, 9, and 19) that were preceded by short deglaciations similar to the Holocene all show downward gas trends (Figures 2a and 2b). These downward trends are consistent with the early anthropogenic hypothesis and not with the natural hypotheses.

As noted earlier, the CO_2, CH_4, δD, and $\delta^{18}O$ trends during stage 15 in Figure 2 based on the $e \sin \omega$ alignments are different from those during the other interglaciations prior to the Holocene. The sequence of isotopic stages from 13 to 15 has long been recognized as unusual. Stage 13 is not a full interglaciation, and stage 14 does not appear to reach a full glacial state [*Lisiecki and Raymo*, 2005; *EPICA Community Members*, 2004]. In addition, within stage 15, the $\delta^{18}O$ trend continued to decrease slowly, before abruptly turning toward more positive (glacial) values (Figure 4). Either ice sheets were still melting throughout the entire stage 15 "interglaciation" or the deep ocean was still warming, or both. Stage 15 should probably be excluded from the comparisons in Figures 2 and 3, although this choice makes little difference in the stacked-average trends shown in Figure 3.

In summary, four climate-related indices dated by three different age models show anomalous Holocene behavior beginning between 7000 and 5000 years ago. Similar findings are also apparent in CO_2, CH_4, and δD trends for stages 5, 7, and 9 at Vostok Station based on the GT4 gas and solid age models [*Petit et al.*, 1999; *Ruddiman*, 2003, 2007]. These anomalous trends contradict natural explanations for late Holocene climate and support early anthropogenic intervention in the climate system. Three alternative methods of aligning Holocene gas trends with those in earlier interglaciations yield results consistent with the results reported above (Appendix A).

These four anomalous late Holocene trends fit known linkages in the climate system. Higher CO_2 and CH_4 values caused by early anthropogenic emissions during the late Holocene would be expected to keep Antarctic air temperatures relatively warm (as confirmed by the δD trends), and relatively warm air temperatures in both hemispheres would be expected to promote relatively warmer deep-ocean temperatures and prevent Northern Hemisphere ice growth (as confirmed by the $\delta^{18}O$ signals and glaciological evidence).

Global climate model simulations add independent evidence that these physical linkages connect the four anomalous trends. An experiment with coupled atmosphere-ocean general circulation models (AOGCMs) [*Kutzbach et al.*, 2011, 2013] examined the difference in temperature responses between the higher observed Holocene CO_2 and CH_4 values and the lower natural levels proposed in the early anthropogenic hypothesis. This experiment simulated a warming of 2.8°C over Antarctica for the higher Holocene gas concentrations, compared to the 2.2°C increase derived by converting the average 14.4‰ δD difference between the Holocene and previous interglaciations in Figure 3c to equivalent temperature using the standard formulation [*Jouzel et al.*, 2003]. The anomalously high late Holocene gas concentrations are consistent with the anomalously warm δD anomaly in Figure 3c.
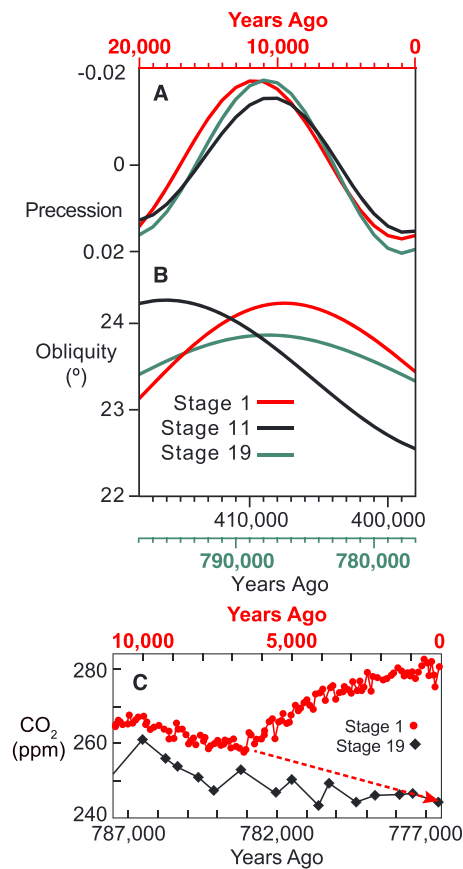
Figure 5. Closest Holocene insolation analog. (a, b) Comparison of orbital changes during interglacial stages 1, 11, and 19. Precession index $e\sin\omega$ and obliquity are from *Berger* [1978]. (c). Stage 19 CO_2 trend [*Luthi et al.*, 2008] compared to Holocene CO_2 values and to (dashed) late Holocene trend predicted by the early anthropogenic hypothesis. Recent analyses shift the CO_2 values upward by ~8 ppm [*Bereiter et al.*, 2015], but retain the same downward trend, in contrast to the late Holocene rise.

The same AOGCM experiment [*Kutzbach et al.*, 2011] simulated a 1.1°C warming of deep-ocean temperature over the 2–4 km depth range in which most of the cores in the benthic isotopic stack [*Lisiecki and Raymo*, 2005] are located. This warming is sufficient to account for about half of the 2.1°C change in $\delta^{18}O$ that would be derived by attributing the entire 0.5‰ $\delta^{18}O$ anomaly in Figure 3d to deep-ocean temperature change, using the standard formulation of 4.2°C per 1‰ $\delta^{18}O$.

But other factors almost certainly influenced this comparison to Holocene $\delta^{18}O$ trends, including formation of new ice sheets during previous interglaciations. New ice sheets probably began to form during the intervals equivalent to the late Holocene in several previous interglaciations [*Ruddiman*, 2007]. General circulation model experiments that omit both industrial era and hypothesized preindustrial CO_2 and CH_4 emissions simulate permanent snow cover in northern Eurasia and North America [*Vavrus et al.*, 2008, 2011]. Because these regions of year-round snow cover are areas of "glacial inception," they imply that part of the $\delta^{18}O$ anomaly in Figure 3d could be due to growth of new Northern Hemisphere ice sheets during previous interglaciations, but not in the late Holocene. In general, lower northern summer insolation during previous interglaciations compared to late Holocene levels would have contributed to the observed 0.5‰ $\delta^{18}O$ difference by aiding both ice sheet formation and cooling of deep and bottom waters.

2.2. Closest Holocene Insolation Analog

Identifying the closest insolation analog to the Holocene among previous interglaciations is a second way to evaluate the natural and early anthropogenic hypotheses. Interglacial stage 11 was originally proposed as the best insolation analog [*EPICA Community Members*, 2004; *Broecker and Stocker*, 2006], but stage 19 is now regarded as the closest analog during the last 800,000 years [*Tzedakis*, 2010; *Tzedakis et al.*, 2012; *Berger and Yin*, 2012]. Stages 11 and 19 both have low-amplitude changes in the $e\sin\omega$ precession index like the Holocene (Figure 5a), but the timing of the obliquity signal relative to $e\sin\omega$ in stage 11 is considerably offset compared to stage 1, while their relative timing in stages 19 and 1 is nearly identical (Figures 5a and 5b). Because obliquity and precession are key sources of climate forcing [*Imbrie et al.*, 1992], both need to be considered in choosing the best analog (Appendix B). Stage 19 differs from stage 1 only in the lower amplitude of the obliquity signal, but by 777,000 years ago, the modern-day time equivalent during stage 19, both precession and obliquity had reached values very similar to those today (Figures 5a and 5b).
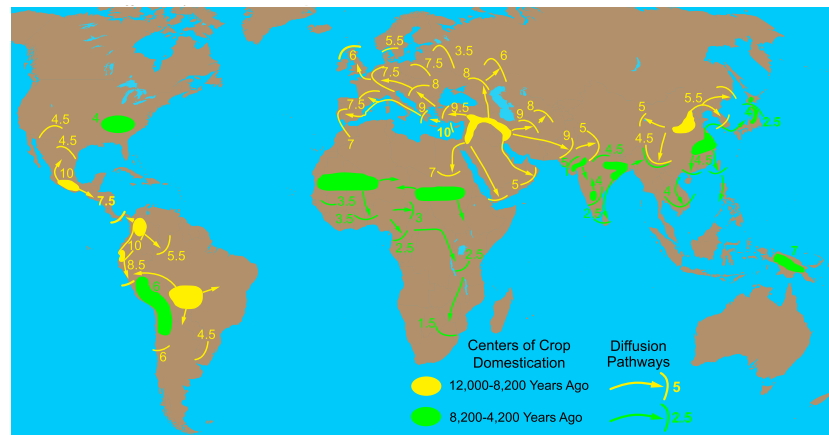
The nearly identical relative timing of obliquity and $e\sin\omega$ changes in stages 1 and 19 minimizes ambiguities in aligning the two interglaciations and allows a meaningful comparison of their greenhouse gas trends. The stage 19 CO_2 signal [*Luthi et al.*, 2008] reached an early-interglacial peak similar to the one at the start of stage 1, after which both fell (Figure 5c). The stage 19 CO_2 trend then continued downward until the modern-day time equivalent 777,000 years ago [*Tzedakis et al.*, 2012], but the stage 1 trend reversed direction after 7000 years ago and increased for the rest of the Holocene. The difference between the 17 ppm stage 19 CO_2 decrease and the 20 ppm late Holocene increase indicates an anthropogenic anomaly of 37 ppm (Figure 5c), close to the 40 ppm anomaly originally proposed [*Ruddiman*, 2003].

Figure 6. The spread of agricultural crops. Domesticated crops originated during the early Holocene from 12,000 to 8200 years ago and in the middle Holocene from 8200 to 4200 years ago [*Fuller et al.*, 2014; *Larson et al.*, 2014]. Numbers along dispersion pathways represent ages in thousands of years.

The largest uncertainty in this comparison is potential errors in the EDC3 gas age model, but *Giaccio et al.* [2015] independently confirmed the basic accuracy of the EDC3 age model for stage 19 by $^{40}Ar/^{39}Ar$ dating of ash layers interbedded in a lake sediment sequence in the Italian Appenines. The sequence also includes the Brunhes/Mautyama paleomagnetic boundary, known to occur in stage 19. The length of the stage 19 interglaciation, as defined by planktic foraminiferal $\delta^{18}O$ variations and $CaCO_3$ percentages in the lake core, closely matches the length derived from the Dome C age model and supports the stage 19 alignment with the Holocene in Figure 5. This dating effort ties the stage 19 interglaciation directly to the astronomical age model and broadly supports the choice of 777,000 years ago as equivalent to the present day.

A GCM simulation [*He et al.*, 2013] showed that stage 19 insolation and greenhouse gas values 777,000 years ago would have produced year-round snow cover (equivalent to glacial inception) in northern Eurasia and North America in the same regions as the late Holocene simulations without anthropogenic greenhouse gases [*Vavrus et al.*, 2008, 2011]. In addition, the presence of millennial-scale oscillations in isotopic records from North Atlantic sediments early in stage 19 adds independent evidence that ice sheets large enough to drive such oscillations had developed by that time [*Tzedakis et al.*, 2012].

CO_2 concentrations in the lower part of the Dome C record have been reanalyzed to evaluate possible biases in gas extraction efficiency using three independent techniques. The new composite record for stage 19 [*Bereiter et al.*, 2015] follows a CO_2 trend parallel to that in Figure 5c [*Luthi et al.*, 2008], but with values shifted upward by an average of about 8 ppm. In any case, the fundamental mismatch between the rising CO_2 trend in the late Holocene and the downward trend in the equivalent part of stage 19 remains intact and continues to indicate anomalous Holocene behavior.

In summary, all of the top-down evidence reviewed above supports the early anthropogenic view that the behavior of the late Holocene climate system is anomalous, while disagreeing with hypotheses that have inferred a natural origin for the Holocene responses. The evidence that supports this conclusion includes the following: the individual trends in CO_2 and CH_4 concentrations and in δD ratios and $\delta^{18}O$ signals shown in Figure 2, the stacked averages of these four trends during previous interglaciations shown in Figure 3, and the gas trends during the closest Holocene insolation analog (interglacial stage 19) shown in Figures 2 and 5.

3. Bottom-Up Evidence

The anomalous rises in CO_2 and CH_4 during the middle to late Holocene (Figures 2 and 3) coincided with the spread of agriculture from major centers of domestication in southwest Asia, China, South Asia, sub-Saharan Africa, Mexico, and tropical South America (Figure 6). In several of these regions, archaeological and paleoecological evidence provides a basis for estimating the magnitude of early agricultural greenhouse gas emissions as a second test of the natural and anthropogenic hypotheses.
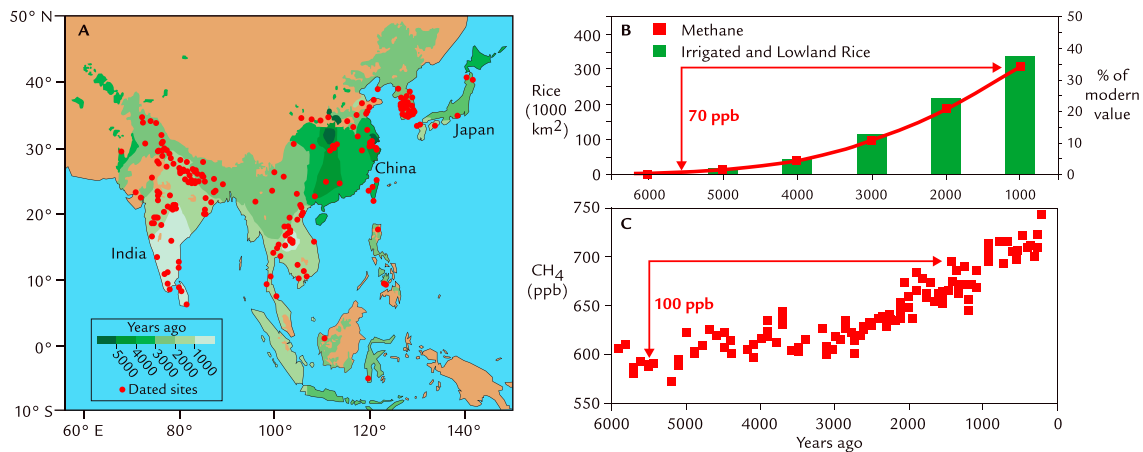
Figure 7. Estimated irrigated rice contribution to atmospheric methane during the late Holocene [*Fuller et al.*, 2011]. (a) Spread of rice farming across southern and southeastern Asia. (b) Estimated area of irrigated rice farming in Asia and contribution to atmospheric CH_4 concentrations, compared to (c) CH_4 concentrations at Dome C [*Monnin et al.*, 2001].

### 3.1. CH₄ From Irrigated Rice and Livestock

Anthropogenic methane emissions during the late Holocene came from several sources, one of which was irrigated rice paddies. *Fuller et al.* [2011] used archaeological and archaeobotanical data to map the spread of irrigated rice from origins in the Yangtze River Valley more than 5000 years ago across the rest of southeastern Asia by 1000 years ago (Figure 7a). They used this mapped spread of irrigated rice to estimate changes in atmospheric CH_4 concentrations based on two assumptions: (1) the spatial density of wet-rice farming grew with the square root of the estimated population size after the first arrival of irrigated rice in each area and (2) modern relationships can be used to convert estimates of total irrigated rice area to CH_4 emissions and enhanced atmospheric CH_4 concentrations between 5000 and 1000 years ago (Figure 7b). With this method, they found that the spread of irrigated rice caused an estimated 70 ppb increase in atmospheric CH_4 by 1000 years ago, a substantial fraction of the 100 ppb increase measured at Dome C (Figure 7c).

The CH_4 rise measured at Dome C is only part of the proposed methane anomaly, because CH_4 values fell during previous interglaciations but did not do so during the late Holocene (Figures 2a and 3a). As a result, the full anthropogenic anomaly proposed for 5000 to 1000 years ago needs to be at least twice as large as the observed increase to confirm the full hypothesis. The spread of CH_4-emitting livestock across Asia and Africa after 5000 years ago (Figure 8) would also have contributed significantly to the growing CH_4 anomaly [*Fuller et al.*, 2011], along with livestock expansion in Europe after initial entry of agriculture from southwest Asia [*Zohary et al.*, 2012; *Colledge et al.*, 2013]. Increased biomass burning of weeds and crop residues would also have added to the anthropogenic CH_4 total as farming spread.

Using a model-based reconstruction of potential natural sources of methane, *Singarayer et al.* [2011] concluded that a significant part of the late Holocene CH_4 rise could have been caused by increased emissions from South America due to greater Southern Hemisphere summer insolation that enhanced monsoon strength in the western Amazon [*Selzer et al.*, 2000]. But the early-interglacial CH_4 responses shown in Figures 2a and 3a raise questions about this conclusion. All previous CH_4 trends fell despite similar or larger increases in Southern Hemisphere insolation forcing [*Berger*, 1978], which should have driven stronger South American monsoons and caused greater CH_4 emissions. It appears that those larger Southern Hemisphere methane contributions in the past were overwhelmed by even larger decreases from shrinking wetlands in the Northern Hemisphere. Given this Northern Hemisphere dominance through previous interglaciations that span 800,000 years, why would southern sources have taken control only during the last 5000 years of the Holocene?

In summary, archaeological evidence of expanding rice irrigation underpins a reconstruction of methane emissions that can explain a substantial part of the observed late Holocene CH_4 anomaly (Figure 7). Contributions from livestock (Figure 8) and other farming activities are likely to add significantly to the anthropogenic total, once they have been quantified.
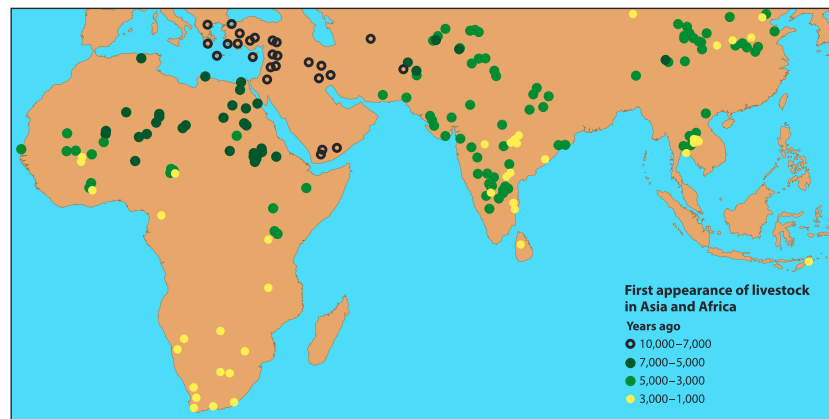
Figure 8. Radiocarbon-dated first appearance of livestock in Asia, Africa, and far southeastern Europe [*Fuller et al.*, 2011] with additions from *Boivin and Fuller* [2009], *Conolly et al.* [2011], and *Arbuckle* [2014].

### 3.2. CO$_2$ From Deforestation

Deforestation is the primary preindustrial source of anthropogenic CO$_2$, with much smaller contributions from early burning of coal and peat [*Ruddiman*, 2003, 2007]. The early spread of agriculture in Figure 6 requires substantial late Holocene deforestation of Eurasia, Africa, and the Americas, consistent with many studies [*Ellis et al.*, 2013]. Two regions—Europe and China—have sufficient paleoecological and/or archaeological evidence to assess the extent of early forest clearance.

Archaeological data document the spread of crops and livestock across Europe, starting 9000 years ago in the southeast and spanning all arable regions by 5500 years ago [*Zohary et al.*, 2012; *Colledge et al.*, 2013]. The arrival and subsequent intensification of agriculture across this naturally wooded continent necessitated forest clearance, and radiocarbon-dated fossil pollen records from sediment cores provide detailed information about changes in vegetation. Pollen data sets for northern and central Europe [*Fyfe et al.*, 2015; *Woodbrige et al.*, 2014] record a shift from forest cover to more open vegetation that began 6000 to 5000 years ago and was complete by the start of the industrial era (Figures 9a and 9b). The Mediterranean region was not included in either analysis, but comparably, early deforestation seems likely because of extensive land use by Greek and Roman civilizations.

Consistent with this evidence, compilations of archaeological site density as a population proxy show abrupt increases after 6000 years ago [*Timpson et al.*, 2014]. These trends lag slightly behind the start of the anomalous CO$_2$ rise (Figures 2b and 3b). Further support for a large early human footprint in Europe comes from mitochondrial DNA analyses [*Gignoux et al.*, 2011] and population modeling studies [*Wirtz and Lemmen*, 2003; *Lemmen*, 2010].

In Britain and France, forests had already been reduced to near-modern levels by 2500 to 2200 years ago [*Fyfe et al.*, 2015; *Woodbrige et al.*, 2014]. Compilations of charcoal abundance in European sediments generally show higher burning levels 3000 years ago than in later times [*Marlon et al.*, 2013]. In addition, analysis of the fire indicator levoglucosan in the NEEM ice core record from Greenland points to increasing amounts of burning until 2500 years ago, followed by a leveling off and then a decrease [*Zennaro et al.*, 2015]. These regional indications of reduced burning could have contributed to the slowing of the CO$_2$ rise after 2500 years ago (Figures 2b and 3b).

Although forest clearance trends in Europe provide support for the anthropogenic explanation of the late Holocene CO$_2$ increase at Dome C, other regions need to be examined to reach a global view. A summary of pollen evidence from east central China [*Ren*, 2007] indicates widespread forest cover until 8000 years ago, followed by a persistent decrease attributed mostly to anthropogenic clearance, especially after 6000 years ago. These pollen records, however, are not adjusted for differential productivity of trees and open vegetation, and making these adjustments would likely reduce estimated forest cover. Also, in Southeast Asia, gradual weakening of the summer monsoon, and the resulting drying effect on vegetation, complicates attempts to isolate the unique effect of clearance by humans.
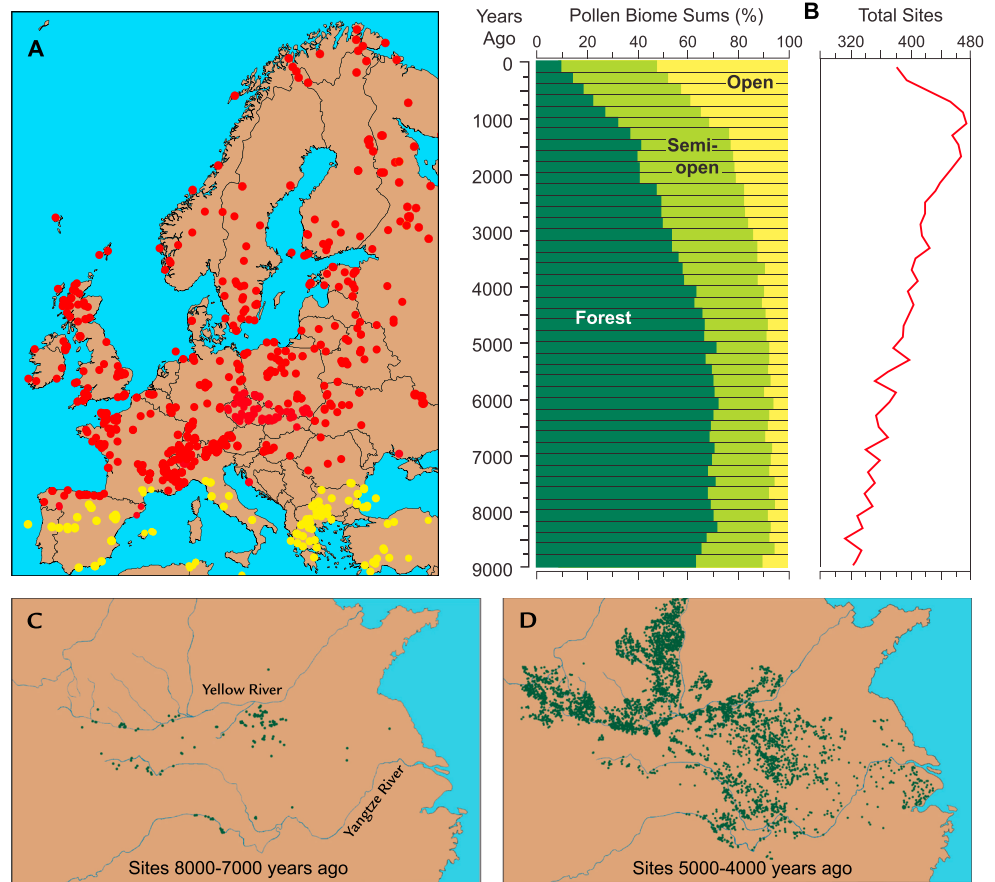
Figure 9. Evidence of early forest clearance and settlement. (a) Locations of cores in the European pollen database. Cores used for pollen summary in Figure 9b shown in red [*Fyfe et al.*, 2015]. (b) Changes in vegetation "pseudobiome" sums for forest, open, and semiopen (mixed forest and open) vegetation. (c, d) Mid-Holocene increase in number of archeological sites in north central China [*Li et al.*, 2009].

Fortunately, an independent source of evidence linked to land cover is available in China. Archaeological sites in central China (Figures 9c and 9d) increased thirtyfold between 8000–7000 and 5000–4000 years ago [*Li et al.*, 2009; *Wagner et al.*, 2013]. This very dense early settlement in central China implies substantial deforestation that would have added to the CO_2 rise after 7000 to 6000 years ago. By 4000 years ago, coal had come into use as a fuel source in the Yellow River Valley because of lack of wood [*Dodson et al.*, 2014]. Deforestation of southern China during the spread of rice agriculture after 5000 years ago (Figure 7a) added to the ongoing CO_2 increase.

In India, sedentary farming and clearance emerged between 5000 and 3500 years ago, with especially rapid settlement expansion on the Deccan Plateau and in the Ganges plains [*Fuller*, 2011; *Kingwell-Banham and Fuller*, 2012]. Studies in all these regions provide ground truth support for large-scale forest clearance coincident with the anomalous rise in CO_2 during the middle and late Holocene.

To assess the effect of humans on the late Holocene CO_2 rise, global forest clearance has to be converted to carbon emissions. Several initial model simulations that explored this link relied on the assumption that the amount of forest cleared and land farmed was tightly linked to population, with clearance per person remaining at about 1 ha throughout the late Holocene [*Pongratz et al.*, 2008; *Strassmann et al.*, 2008; *Stocker et al.*, 2011]. Because (estimated) populations were small in the millennia before the industrial era, these analyses inevitably simulated little early deforestation anywhere.

However, in direct contradiction to the assumption of small, nearly constant clearance per person, historical data [*Buck*, 1937; *Chao*, 1986; *Ellis and Wang*, 1997] show that per capita use of cultivated land in China declined by a factor of 4 after 2000 years ago (Figure 10a), and historical sources in Europe [*Kaplan et al.*, 2009, 2011]
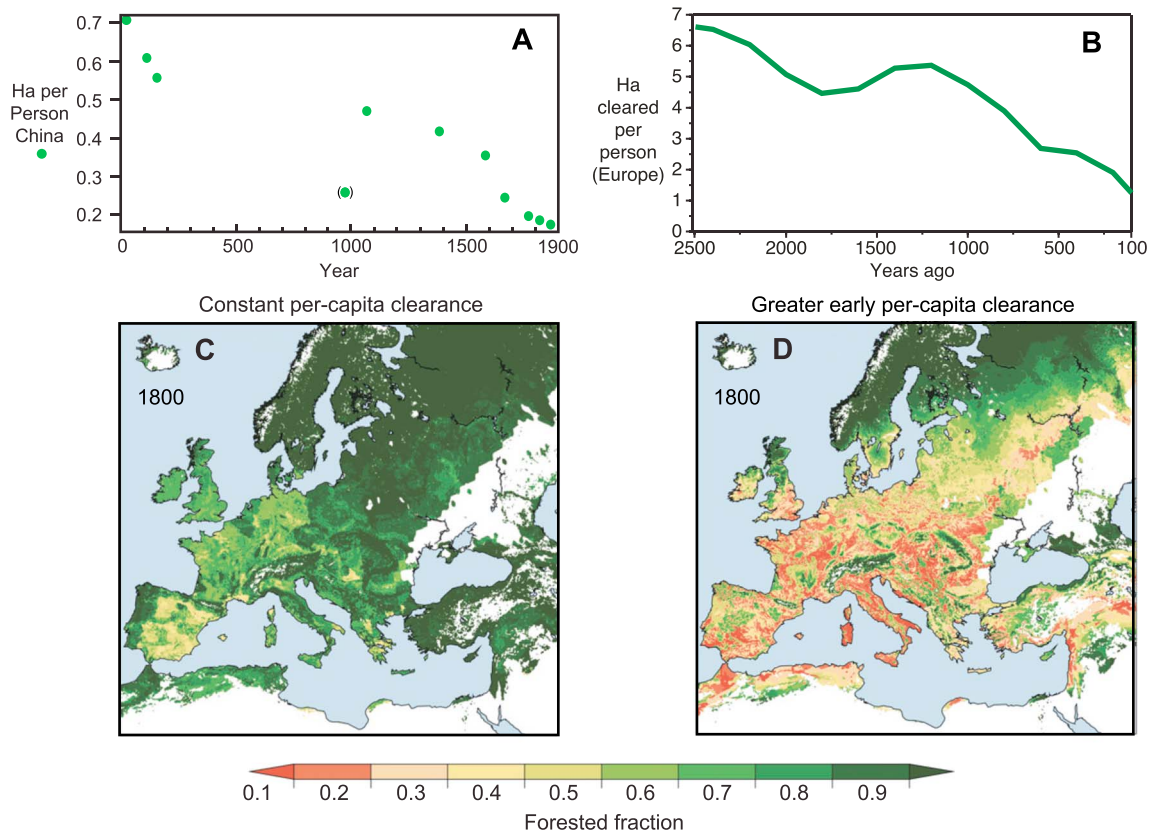
Figure 10. Effect of per capita clearance on land use reconstructions. (a) Per capita decrease of cultivated cropland in China [*Buck*, 1937; *Chao*, 1986; *Ruddiman et al.*, 2011]. (b) Per capita decrease of area deforested for crops, pastures, and other anthropogenic uses in Europe [*Kaplan et al.*, 2011]. (c, d) Simulated European forest extent at 1800 [*Kaplan et al.*, 2009], assuming small constant per capita Holocene land use (Figure 10c) and the large early per capita clearance shown in Figure 10b.

indicate a similar fourfold decrease in per capita forest clearance during that time (Figure 10b). This historical evidence supports the insight of Ester Boserup that early land use was inefficient and required large amounts of land but gradually became more "intensive" as agricultural technologies improved during the Holocene [*Boserup*, 1981].

The KK10 land use model simulation of *Kaplan et al.* [2011] is calculated from population and land use intensity [*Kaplan et al.*, 2009]. The simulation indicates much greater deforestation during the millennia preceding the industrial era (Figure 10d), in basic agreement with the European pollen evidence for predominantly preindustrial clearance (Figure 9). In contrast, the reconstruction that assumed small constant per capita clearance during preindustrial time shows 40–80% forest cover still persisting in western and central Europe by the year 1800 (Figure 10c). This latter simulation faces a major problem. Explaining the much reduced forest cover that exists in Europe today would then require massive deforestation during the last 200 years, but historical data instead show pervasive reforestation in western and central Europe since 1800, not deforestation [*Mather and Needle*, 2000]. Simulations that assume small constant per capita clearance cannot explain the small present-day forest cover in Europe.

The available paleoecological and archaeological evidence, as well as the historically based land use model simulation, support the early anthropogenic view that preindustrial forest clearance was very large, rather than the opposing view that early clearance was limited. The total amount of estimated anthropogenic carbon emitted in the simulations based on the constant per capita land use assumption [*Pongratz et al.*, 2008; *Strassmann et al.*, 2008; *Stocker et al.*, 2011] averages 210 Gt, with ~70 Gt of this total during preindustrial time and ~140 Gt during the industrial era. In comparison, the historically based KK10 simulation described earlier estimated total emissions of ~450 Gt C, with 343 Gt during preindustrial time and 108 Gt in the industrial era.

Several factors account for most of this very large difference in estimates. First, the estimates based on constant per capita clearance missed much of the preindustrial clearance. Second, those estimates included only cultivated land and pastures in active use. In contrast, the KK10 estimate also includes other kinds of cleared land: areas of shifting cultivation (land where crops are planted infrequently), rarely used pastures, degraded and abandoned land, and steep hillsides that were deforested but not used for agriculture.

In addition, models that simulated small early anthropogenic emissions are vulnerable to the challenge that their estimates of early populations were too low. These land use reconstructions assumed more or less geometric rates of population increase through the millennia prior to the historical era, with the fractional rate of population increase held nearly constant because environmental constraints on populations were assumed to have remained stable.

In contrast, logistic growth models (widely used in population ecology) assume that fractional growth rates of organisms and ecosystems are faster initially when resources are abundant and then slow as resources are depleted. In the case of early agriculture, rapid early population growth was likely favored by the ready availability of fertile well-watered valley soils but slowed as farmers increasingly toiled on higher, less fertile terrain with less reliable water. Reconstructions based on this logistic assumption and other constraints (including emerging technologies) show much larger fractional population growth rates in early agricultural history than the geometric models [*Wirtz and Lemmen*, 2003; *Lemmen*, 2010], consistent with the evidence from mitochrondrial DNA analyses [*Gignoux et al.*, 2011] and syntheses of ^{14}C-dated archaeological sites [*Timpson et al.*, 2014] noted previously.

For a larger perspective, the preindustrial release of 340 Gt C based on the KK10 simulation [*Kaplan et al.*, 2011] can be viewed in the context of estimated global terrestrial carbon budget at the start of the industrial era [*Horel and Geisler*, 1996]. Aboveground carbon in 1800 amounted to 610 Gt, while belowground carbon was estimated at 1560 Gt, mostly in slow-turnover deep carbon, with roughly 200 Gt C of that amount in shallow fast-overturning carbon such as litter and roots. The total amount of aboveground and other fast-overturning carbon effectively in contact with the preindustrial atmosphere was thus ~810 Gt. Adding this 810 Gt C to the *Kaplan et al.* [2011] estimate of 340 Gt emitted prior to the industrial era implies that the original (natural) amount of carbon 7000 years ago would have been 1150 Gt (or more because northern monsoons were stronger) and that ~30% (340 Gt) of that original total was removed by preindustrial agriculture.

In summary, the available bottom-up evidence supports the hypothesis of large-scale early anthropogenic effects on atmospheric greenhouse gas concentrations. Methane emissions from irrigated rice account for a substantial part of the increase in atmospheric CH_4 between 5000 and 1000 years ago, and archaeological data mapping the spread of livestock across Asia, Africa, and Europe are likely to add significantly to that total. Pollen syntheses and other data from Europe document early deforestation that would have made a substantial regional contribution to the CO_2 increase that began near 6500 years ago, and pollen and archaeological syntheses provide a semiquantitative indication of similarly early deforestation in north central China. Although all of this evidence is favorable to the early anthropogenic hypothesis, quantitative estimates of methane emissions from livestock, as well as ground truth evidence on the timing of deforestation and carbon emissions in other regions, are needed to clarify the emerging picture of large early anthropogenic effects.

4. Late Holocene Carbon Budgets and the $\delta^{13}CO_2$ Index

As shown above, every top-down analysis of the late Holocene CO_2 record points to anomalous preindustrial emissions of carbon from a source plausibly interpreted as anthropogenic. The one comprehensive bottom-up synthesis of deforestation now available (for Europe) supports this interpretation and is consistent with a land use simulation of large preindustrial clearance based on historical records of per capita land use. Archaeological data from China also imply large early clearance.

4.1. Does the Weak $\delta^{13}CO_2$ Signal Invalidate the Early Anthropogenic Hypothesis?

A potential argument against the early anthropogenic explanation of the late Holocene CO_2 increase centers on the $\delta^{13}C$ trend recorded in ice core CO_2 signals over the last 7000 years [*Elsig et al.*, 2009]. This signal places a constraint on the total net release of ^{12}C-rich terrestrial carbon to the atmosphere, after allowance for exchanges with other carbon reservoirs, including the large deep-ocean reservoir. The small negative
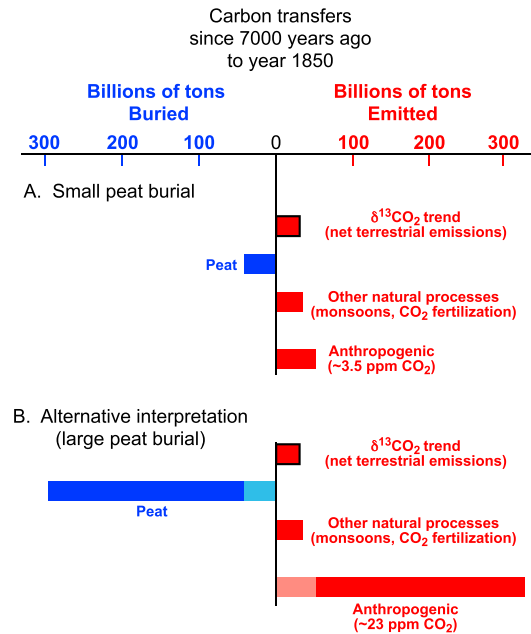
Figure 11. Two mass balance estimates of carbon transfers among major reservoirs during the last 7000 years: (a) based on assumption of small peat burial [*Elsig et al.*, 2009] and (b) based on larger peat burial [*Yu*, 2011; *Ruddiman et al.*, 2011].

amplitude of the $\delta^{13}CO_2$ trend during the last 7000 years (−0.05‰) indicates small net terrestrial emissions (anthropogenic and other).

Elsig and colleagues ran an analysis that satisfied both the 20 ppm CO_2 increase and the small $\delta^{13}CO_2$ trend. They claimed that their analysis "… render[s] untenable suggestions that CO_2 emissions from anthropogenic land use changes caused the later CO_2 rise…," but this conclusion has not held up to scrutiny. The major problem is that their mass balance analysis proposed to account for the −0.05‰ $\delta^{13}CO_2$ change by assuming that 40 Gt of carbon was buried in peatlands during the last 7000 years (Figure 11a), but this estimate lies far below a comprehensive synthesis that indicated 250–300 Gt of carbon burial in global peatlands during that time [*Yu*, 2011; *Gorham*, 1991]. Subsequently, several members of the Bern group, with Yu as co-author, simulated much larger late Holocene peat accumulation using a dynamic global vegetation model with a peatland submodule [*Spahni et al.*, 2013]. This later study is consistent with the larger estimate of peat carbon burial from *Yu* [2011].

This much greater burial of ^{12}C-enriched carbon in global peats must be balanced by some 300 billion tons of additional terrestrial carbon emissions to maintain mass balance and account for the small net $\delta^{13}CO_2$ trend [*Ruddiman et al.*, 2011]. Anthropogenic deforestation is one of the several possible sources of greater terrestrial carbon emissions during the last 7000 years that could fill this gap. Rather than solving for deforestation emissions, *Elsig et al.* [2009] made an a priori choice of 50 Gt of anthropogenic carbon from deforestation based on a previous land use simulation [*Stocker et al.*, 2011]. But, as noted above, that simulation relied on the flawed assumption of small, nearly constant preindustrial land use. The more realistic estimate of 300 Gt C of preindustrial deforestation in Figure 11b would restore mass balance and also falls close to the preindustrial estimate of 340 Gt C from *Kaplan et al.* [2011].

Early anthropogenic deforestation is only one possible source of additional terrestrial carbon (or burial) during the last 7000 years. Changes in other large reservoirs are also possible, including release (or storage) of terrestrial carbon in nonpeat permafrost [*Zimov et al.*, 2009] and exhumation (or burial) of terrestrial carbon in river floodplains and deltas [*Hoffman et al.*, 2013]. In view of the underestimate of carbon burial in peats and these uncertainties about other potentially significant carbon sources and sinks, the $\delta^{13}CO_2$ record cannot be used to "render untenable" the large amount of early deforestation proposed in the anthropogenic hypothesis.

Several recent investigations have continued to explore changes in $\delta^{13}CO_2$ and CO_2 during previous interglaciations. *Schneider et al.* [2013] noted that the $\delta^{13}CO_2$ trend in stage 5 was not markedly different from that in the Holocene, despite the obvious absence in stage 5 of an anthropogenic overprint. This evidence could be taken to imply a minimal early anthropogenic overprint during the Holocene as well. However, the carbon sinks and sources that are uncertain during the Holocene are even more difficult to constrain during stage 5, which was also a time of far greater summer/winter insolation extremes, with ice sheets developing between 120,000 and 116,000 years ago (the late Holocene time equivalent). Given these complexities, the stage 5 $\delta^{13}CO_2$ data are not a strong basis for assessing the Holocene anthropogenic impact.

Schneider et al. [2013] also noted that the timing of the late Holocene CO_2 peak is delayed compared to the one in interglacial stage 5, and they proposed a natural explanation: "…Termination I is special since it is characterized by the intermittent cooling during the YD [Younger Dryas] event, which was also accompanied by an intermittent decline in terrestrial carbon storage…." "Accordingly, we attribute the increasing CO_2

trend later in the Holocene and the lack of such a trend during MIS 5.5 to the effect of carbonate compensation in response to the occurrence of the YD cold anomaly…." Yet to be demonstrated is a plausible physical/chemical mechanism by which a 1500 year deglacial oscillation could have shifted a natural CO_2 peak some 10,000 years later in time from its normal early-interglacial position.

Simulations with carbon/climate models have also been used to explore the merits of the natural and early anthropogenic hypotheses. A recent attempt [*Ganopolski and Brovkin*, 2015] coupled the CLIMBER-2 model to a biogeochemical submodule, with both forced by orbital variations and a reconstructed sea level signal. Although this simulation reproduced the general features of the CO_2 record over the last 400,000 years, it did not perform well during early-interglacial intervals. Instead of capturing the swift rises to well-marked CO_2 peaks at the start of the Holocene and stages 5, 7, and 9, the model simulated slow CO_2 rises to muted peaks that occurred many thousands of years later. In short, their model simulated upward trends early in pre-Holocene interglaciations, rather than the downward ones observed in ice core records (Figures 2b and 3b). A related effort by *Kleinen et al.* [2015] failed to simulate the observed CO_2 rise of the last 3000 years using only natural factors and invoked substantial anthropogenic emissions.

Ruddiman [2008] noted that attempts to reproduce early-interglacial CO_2 trends face a major challenge: "No model has yet reproduced both the upward gas trends during the Holocene and the downward gas trends in previous interglaciations" (without using Holocene anthropogenic intervention). Years later, that challenge is still unmet.

4.2. Climatic Role of Carbon Burial in Peat During Interglaciations

Carbon burial in peat during the late Holocene and equivalent times in previous interglaciations has important implications both for the natural end of warm interglacial climates and for the early anthropogenic hypothesis. Carbon burial in peat during this interglaciation is assumed to have been largely natural in origin, because it began 13,000 to 12,000 years ago, long before the emergence of major anthropogenic effects. It then continued at an uninterrupted but slowly decreasing rate as agriculture spread and the anomalous greenhouse gas trends emerged [*Yu*, 2011]. The dynamic wetland model of *Kleinen et al.* [2012, 2015] simulated similar rates of peat accumulation during previous interglaciations under naturally warm conditions.

Considered as a single isolated factor, these large interglacial accumulations of carbon in peat should have gradually cooled global climate. *Klinger et al.* [1996, and references therein] proposed that late-interglacial carbon burial in peats would have reduced atmospheric CO_2, cooled climate, and aided glacial inception. Their paper was published a few years before CO_2 data from Antarctica were published, but their hypothesis later turned out to be consistent with the (natural) downward CO_2 trends early in previous interglaciations. It also matched the CO_2 decrease from 10,000 to 7,000 years ago, but not the anomalous (anthropogenically overprinted) increase during the last 7000 years (Figures 2b, 3b, and 5c). This analysis does not refute the view that carbon burial in the deep ocean is important in CO_2 changes, but carbon burial on land in peat and permafrost [*Zimov et al.*, 2009; *Yu*, 2011; *Schneider van Deimling et al.*, 2012] cannot be dismissed as a factor in late-interglacial global carbon budgets.

The large accumulation of carbon in boreal peat during recent millennia also ties in directly with the early anthropogenic hypothesis. In the original hypothesis, *Ruddiman* [2003] proposed a 40 ppm anthropogenic CO_2 anomaly for the late Holocene, with just over half accounted for by the CO_2 increase observed in ice cores, and the rest reflecting the fact that CO_2 fell throughout previous interglaciations, but not during the last 7000 years of the current interglaciation. This latter part of the proposed anomaly is also based on observations but indirectly by inference from the difference in trends between the late Holocene and previous interglaciations. Carbon burial in peat during the late Holocene thus contributed to this second (inferred) part of the proposed anthropogenic anomaly.

4.3. Late Holocene CO$_2$ Anomalies and Carbon Budgets

Although not a refutation of the early anthropogenic hypothesis, the small negative $\delta^{13}CO_2$ signal during the last 7000 years still places an important constraint on the late Holocene global carbon budget. The $-0.05‰$ trend allows only ~36 Gt of net emissions of ^{12}C-rich terrestrial carbon during that interval [*Elsig et al.*, 2009], equivalent to less than a 3 ppm CO_2 increase if fully equilibrated with the ocean carbon reservoir at 1 ppm

Table 1. Late Holocene CO_2 Anomalies and Carbon Budgets (1 ppm CO_2 = 14.2 Gt of Carbon)[a]

Environmental Process	(A) Contribution to 40 ppm Anomaly	(B) Contribution to 20 ppm Increase	(C) Effect on $\delta^{13}CO_2$ and Gt C Burial
Direct emissions (deforestation)	24 ppm/340 Gt[b]	24 ppm/340 Gt[b]	24 ppm/340 Gt[b]
Peat burial	0 ppm/Gt C	−21 ppm/−300 Gt[c]	−21 ppm/−300 Gt[c]
Direct emissions minus peat burial	24 ppm/340 Gt	~3 ppm/36 Gt	~3 ppm/36 Gt
Ocean feedbacks			
CO_2 solubility	6 ppm/84 Gt[d]	6 ppm/84 Gt[d]	0
Southern Ocean	5–15 ppm/71–213 Gt[e]	5–15 ppm/71–213 Gt[e]	0
Overall total	35–45 ppm/497–639 Gt	14–24 ppm/199–341 Gt	~3 ppm/36 Gt C
Budget required	40 ppm[f]	20 ppm	~3 ppm

[a]Estimates in table cover the interval from 7000 years ago to the start of the industrial era.
[b]*Kaplan et al*. [2011].
[c]*Yu* [2011].
[d]*Kutzbach et al*. [2011] (scaled down from 0.88°C for 40 ppm CO_2 anomaly).
[e]*Simmons et al*. [2013].
[f]*Ruddiman* [2003].

CO_2 = 14.2 Gt C [*Joos et al.,* 2004]. This means that more than 17 ppm of the observed 20 ppm rise must have come from the ocean with a neutral ^{13}C composition that had no effect on the $\delta^{13}CO_2$ index.

The two natural hypotheses, delayed carbonate compensation and coral reef building (section 1), could meet this constraint by calling on releases of isotopically neutral ocean carbon to explain the CO_2 increase. But all of the top-down evidence reviewed in section 2 indicates that neither of the natural hypotheses is consistent with the decreasing CO_2 trends in equivalent parts of past interglaciations. Not one of the six valid interglacial orbital analogs—stages 5, 7, 9, 11, 17, nor 19—shows a CO_2 increase, even though conditions were similar to those in the Holocene, with rapid deglaciations ending, forests moving north, and sea level rising and then stabilizing. These prior interglaciations show no sign of natural releases of large amounts of oceanic carbon.

The alternative explanation—the early anthropogenic hypothesis—faces a major challenge. It has to account not just for the predominantly nonterrestrial contribution of more than 17 ppm to the observed 20 ppm CO_2 rise but also for the proposed 40 ppm total anthropogenic anomaly [*Ruddiman*, 2003]. A possible solution to this challenge, based on the evidence presented above, is shown in Table 1.

The starting point for this analysis is the estimate of 340 Gt of early anthropogenic terrestrial carbon emissions from the KK10 land use simulation of *Kaplan et al.* [2011]. These emissions would amount to a 24 ppm increase in atmospheric CO_2 if fully equilibrated with the ocean and other carbon reservoirs. Other direct anthropogenic emissions from preindustrial burning of coal and peat, roughly estimated at 1–2 ppm [*Ruddiman*, 2003, 2007], are ignored.

Most of the 24 ppm (340 Gt) of deforestation carbon emissions does not show up in the 20 ppm CO_2 rise because of the offsetting 300 Gt of natural carbon burial in global peats [*Yu*, 2011]. However, the 24 ppm CO_2 contribution from deforestation still counts toward the proposed early anthropogenic anomaly of 40 ppm because it results from past human activity, whereas the burial of carbon in peat is considered nonanthropogenic.

This estimated 24 ppm deforestation effect on CO_2 emissions, combined with the estimated 310 ppb increase from early anthropogenic CH_4 emissions, did not cause an increase in atmospheric and oceanic temperature, but rather prevented most of a cooling that would otherwise have occurred, as indicated by the previous interglacial trends in Figures 2c/2d and 3c/3d. This "anomalously warmer" late Holocene ocean emitted CO_2 that would have stayed in the ocean if a natural cooling had occurred. These releases are CO_2 feedbacks that add to the anthropogenic total from direct emissions [*Ruddiman*, 2007].

In this (relatively) warmer ocean, decreased CO_2 solubility resulted in an anomalous CO_2 release to the atmosphere. The previously mentioned AOGCM simulation of *Kutzbach et al.* [2011, 2013], which assessed the effect of the full proposed 40 ppm CO_2 anomaly and the 310 ppb CH_4 anomaly, found a whole-ocean warming of 0.88°C, which would cause a CO_2 solubility release of 8–9 ppm. Scaled down linearly to the 24 ppm estimate of direct CO_2 emissions from *Kaplan et al.* [2011] and still allowing for the full 310 ppb anomaly for CH_4, the CO_2 solubility release would be 6 ppm. Added to the 24 ppm of direct emissions, this would bring the early anthropogenic (preindustrial) total to 30 ppm. It would also account for 6 ppm of the
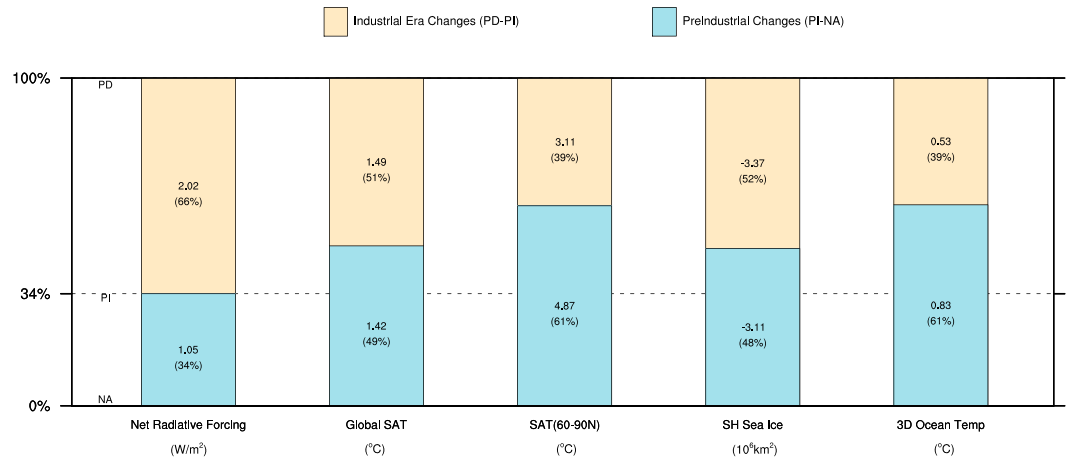
Figure 12. Annual average changes in greenhouse gas radiative forcing and in the responses of four climate indices (global surface air temperature, SAT; SAT for 60 N–90 N; Southern Hemisphere sea ice area; and three-dimensional average ocean temperature [from *Kutzbach et al.*, 2011, 2013]). Changes from preindustrial time to the industrial era are also expressed as relative percentages. PD (present-day) simulation based on the late 1990s greenhouse gas values. PI (preindustrial) simulation uses values from 1800. NA ("no anthropogenic") simulation omits both observed industrial era gas increases and preindustrial increases proposed by *Ruddiman* [2003].

observed 20 ppm CO_2 increase during the last 7000 years without having any ^{12}C negative effect on the $\delta^{13}CO_2$ signal because of the neutral $\delta^{13}C$ signature of oceanic carbon. The $\delta^{18}O$ trends in Figures 2d and 3d provide independent support that this proposed solubility feedback actually occurred: the late Holocene deep ocean remained anomalously warm compared to the cooling in previous interglaciations.

The second oceanic CO_2 feedback mechanism calls on greater CO_2 venting to the atmosphere from a Southern Ocean kept anomalously warm compared to the natural cooling that would have occurred without anthropogenic intervention. The Southern Ocean has long been recognized as an important player in atmospheric CO_2 variations because of the effects of its sea ice cover and ocean circulation on exchanges of oceanic CO_2 with the atmosphere. Processes in this region are complex, and coupled atmosphere-ocean models with interactive biogeochemical modules are required to assess this feedback.

Simmons et al. [2013], using the University of Victoria Earth System Climate Model coupled to the McGill "Green" model, analyzed the last 8000 years, allowing the atmospheric CO_2 concentration to evolve freely in response to Holocene orbital forcing. For a range of experiments, atmospheric CO_2 fell by 5 to 15 ppm, with none of the simulations producing a CO_2 increase. These CO_2 decreases occurred because orbital forcing drove a natural cooling that led to expanded sea ice cover and reduced CO_2 ventilation to the atmosphere. The 10 ppm range of CO_2 decreases in the various experiments reflects different treatments of Antarctic ice shelves. Uncertainties connected with this Southern Ocean mechanism (and other possible feedbacks linked to ocean circulation) are greater than for the CO_2 solubility mechanism.

Consistent with these simulations, Antarctic δD trends during pre-Holocene interglaciations show a natural shift toward more negative (colder) values (Figures 2c and 3c). In contrast to these natural trends, Holocene δD values remained warm, which would have allowed greater CO_2 exchanges with the atmosphere to continue. Both the model simulations and ice core δD trends indicate that Southern Ocean feedback contributed to the early anthropogenic CO_2 anomaly.

This natural 5–15 ppm CO_2 decrease that did not happen during the Holocene can be counted as another contribution to the proposed 40 ppm CO_2 anomaly, bringing the estimated total to 35–45 ppm (Table 1). And it adds 5–15 ppm to the observed 20 ppm CO_2 increase, bringing the estimated total to 14–24 ppm, while not adding any ^{12}C-enriched carbon to the $\delta^{13}CO_2$ signal.

The simulated temperature effects in the AOGCM simulation of *Kutzbach et al.* [2011, 2013] indicated an enhanced climate sensitivity to the lower greenhouse gas concentrations proposed in the early anthropogenic hypothesis relative to those of the present day (Figure 12). The larger relative preindustrial responses

despite lower radiative forcing from greenhouse gases indicate enhanced global climate sensitivity at lower gas concentrations (colder climates). This result provides further insight into the potential importance of the middle to late Holocene increases of greenhouse gases.

The combined effects of direct greenhouse gas emissions [*Kaplan et al.*, 2011], CO_2 solubility feedback [*Kutzbach et al.*, 2011], and Southern Ocean CO_2 feedback [*Kutzbach et al.*, 2011; *Simmons et al.*, 2013] meet the carbon budget and $\delta^{13}CO_2$ constraints listed earlier (Table 1). Column A shows that direct terrestrial emissions and related ocean feedbacks can satisfy the full 40 ppm CO_2 anomaly proposed by *Ruddiman* [2003]. Column B shows that the smaller net 20 ppm CO_2 increase observed in ice cores results from partial cancellation of the full anthropogenic total by carbon burial in peats. Column C shows that the small net influence of terrestrial carbon on the $\delta^{13}CO_2$ record of the last 7000 years results from carbon burial in peat offsetting most direct terrestrial anthropogenic emissions and from the large contribution of $\delta^{13}C$-neutral ocean carbon from feedback processes.

Several of the estimates in Table 1 are based on published studies that will obviously be subject to future scrutiny and likely revision, so this mass balance reckoning is tentative. Still, these currently available estimates provide a possible explanation for how early anthropogenic emissions altered late Holocene climate.

4.4. Conclusions

The late Holocene stands apart from equivalent intervals in other interglaciations of the last 800,000 years by registering greenhouse gas increases instead of decreases and in showing regional temperature stability in most regions instead of a shift toward glacial conditions (section 2). These anomalous responses implicate anthropogenic interference in the climate system. Independent ground truth estimates of CH_4 and CO_2 emissions sufficient to account for substantial parts of these inferred anomalies come from syntheses of archaeological and paleoecological data and from land use modeling (section 3). After more than a decade of debate over whether late Holocene climate was natural or anthropogenic, the convergence of evidence from these several branches of scientific inquiry points to a major anthropogenic influence.

Appendix A: Different Interglacial Alignments

The method used to align the Holocene with previous interglaciations is an important issue in the debate over the early anthropogenic hypothesis.

Aligning on precession (*esinω*). The hypothesis aligned interglaciations on the first maximum in *esinω*, coincident with the first minimum in caloric summer half-year insolation in the Northern Hemisphere. The first maxima in the precession index *esinω* fall on or very close to the first Northern Hemisphere minima in caloric summer insolation (Table A1). This index, favored by *Milankovitch* [1941], sums the 182 days of the year for which insolation at the critical latitude of 65°N is higher than the other 182 days. It reduces the overwhelming dominance of orbital precession on insolation changes calculated at fixed daily, monthly, or seasonal intervals, and it incorporates some of the influence of changes in orbital obliquity.

This alignment method can be used to examine greenhouse gas trends in previous interglaciations during the intervals equivalent to the late Holocene, with special attention to the late Holocene when gas trends rose (text Figures 2a and 2b and Table A2). In all seven previous interglaciations, CH_4

Table A1. Ages of First Caloric Summer Half-Year Northern Insolation Minima and First Precessional (*esinω*) Insolation Maxima in the Holocene (Stage 1) and Previous Interglaciations

Interglacial Stage	*esinω* Insolation Minimum (Years Ago)	Caloric N. Summer Maximum (Years Ago)
1	500	−1500
5	117,000	116,500
7	231,000	231,000
9	323,500	322,000
11	398,500	398,000
15	610,000	610,000
17	683,000	683,000
19	777,500	777,000

Table A2. CH_4 and CO_2 Trends During Previous Interglaciations: $esin\omega$ Alignment[a]

Interglaciation	CH_4 Trend	CO_2 Trend
Stage 5	decrease	decrease[b]
Stage 7	decrease	decrease
Stage 9	decrease	decrease
Stage 11	decrease	decrease[b]
Stage 15	decrease	increase[c]
Stage 17	decrease	decrease
Stage 19	decrease[b]	decrease

[a]Natural explanations predict CH_4 increases (like that in the current interglaciation). Anthropogenic explanation predicts CH_4 decreases (unlike the increase in the current interglaciation).
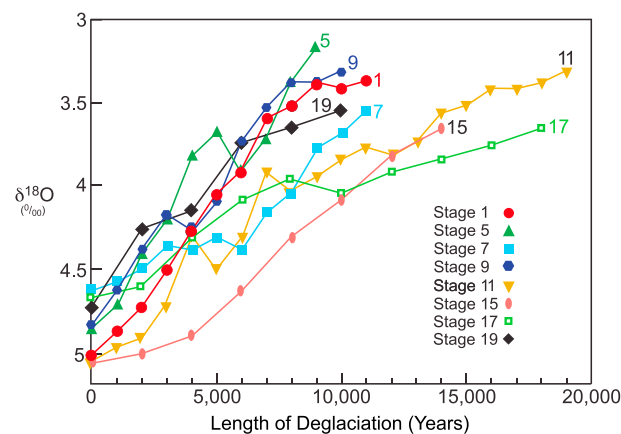[b]Small-amplitude trend.
[c]Ice volume ($\delta^{18}O$) trend is anomalous.

concentrations fell during the late Holocene equivalent intervals, and CO_2 trends decreased for six of the seven interglaciations by varying amounts (see text Figures 2a and 2b). Overall, this alignment method indicates that the late Holocene CO_2 and CH_4 increases were anomalous compared to previous interglaciations. Because anthropogenic emissions could not have been a factor in previous interglaciations, the anomalous late Holocene gas increases have been interpreted as anthropogenic [*Ruddiman*, 2003; *Ruddiman et al.*, 2011].

Other methods of aligning gas trends during the Holocene and previous interglaciations are possible. This appendix explores three other ways.

Deglaciation Alignments. Another method used to compare interglacial isotopic stage 11 with the Holocene focuses on the preceding deglaciations. *EPICA Community Members* [2004] and *Broecker and Stocker* [2006] aligned the rapid deuterium/hydrogen (δD) and CO_2 rises that occurred early in the stage 12/11 deglaciation with the similarly rapid rises early in the pre-Holocene deglaciation.

Glacial-interglacial cycles are usually defined by changes in the $\delta^{18}O$ ratio. The deglaciations that precede all interglacial intervals can be aligned using the benthic foraminiferal oxygen isotope signals in the global marine stack of *Lisiecki and Raymo* [2005]. The onsets of the terminations are marked by relatively well-defined $\delta^{18}O$ decreases (Figure A1). The ends of some deglaciations are more gradual, with decreasing $\delta^{18}O$ values that gradually approach full interglacial levels. The deglaciations plotted in Figure A1 are truncated at the point that the $\delta^{18}O$ values lie within the range of uncertainty of full interglacial values. Four earlier interglaciations (stages 5, 7, 9, and 19) are preceded by short deglaciations that last 9,000 to 11,000 years, similar to the 10,000 year deglaciation that preceded the Holocene. The other three deglaciations lasted 14,000 to 20,000 years, considerably longer than the one preceding the Holocene.

The ages of the start and end of all eight deglaciations are listed in Table A3.

Aligning on the start of deglaciations. The levels when the deglaciations began (Table A3) can be used to align the subsequent interglaciations. This alignment method produces the individual CH_4 and CO_2 trends plotted in Figure A2.

The gas trends during the previous interglacial intervals equivalent to the late Holocene vary widely. The four interglaciations preceded by short deglaciations like that prior to the Holocene (stages 5, 7, 9, and 19) have downward CO_2 and CH_4 trends during the times equivalent to the late Holocene (Table A4). The three interglaciations preceded by long deglaciations

Figure A1. Deglacial $\delta^{18}O$ trends preceding the Holocene and seven previous interglaciations, aligned on the initial $\delta^{18}O$ decreases at the start of the deglaciations [*Ruddiman et al.*, 2011].

Table A3. Start and End of Deglaciations Based on *Lisiecki and Raymo* [2005]

Interglacial Stage	Start Years Ago	End Years Ago
1	17,000	7,000[a]
5	135,000	126,000
7	252,000	241,000
9	341,000	331,000
11	431,000	412,000
15	631,000	610,000[b]
17	718,000	700,000
19	794,000	784,000

[a]Based on glacial geologic evidence of the final melting of the Laurentide ice sheet.
[b]$\delta^{18}O$ decrease slows at 615,000 years ago but continues throughout stage 15.

(stages 11, 15, and 17) have variable gas trends during the intervals equivalent to the Holocene. However, the latter three cases do not qualify for this comparison because the intervals supposedly equivalent to the Holocene interglaciation fall entirely on the preceding deglaciations.

With the three nonqualifying interglacial comparisons (stages 11, 15, and 17) omitted, all four remaining interglaciations show downward CO_2 and CH_4 trends (Table A4), and the stacked-average CH_4 and CO_2 signals trend steadily downward (Figure A3). In both cases, the stacked averages fall to values well below those of the late preindustrial Holocene.

The downward CO_2 and CH_4 trends in the four qualifying interglaciations and their stacked averages provide no support for the rising trends that would be expected for natural explanations of the late Holocene trends.

Aligning on the end of the previous deglaciations. The ends of the preceding deglaciations (Table A3) can also be used to align the subsequent interglaciations. This method avoids complications of deglaciations that vary widely in duration, and it uses a level that lies closer in "equivalent time" to the Holocene CO_2 and CH_4 rises. In this comparison, downward CH_4 trends predominate during previous interglaciations (Table A5). Three interglaciations show downward CO_2 trends, and stages 15 and 17 show increases. The slow $\delta^{18}O$ decrease throughout stage 15 makes it difficult to define the end of that deglaciation.

The stacked averages for the CH_4 and CO_2 signals during the previous interglacial equivalents of the late Holocene are plotted in Figure A4. The downward trends are very similar whether or not stage 15 is included in the stack. The CO_2 and CH_4 concentrations fall to levels well below those of the late preindustrial Holocene.

Using the end of previous deglaciations to align the subsequent interglaciations yields mainly downward CO_2 and CH_4 trends, contrary to natural explanations for the late Holocene increases.
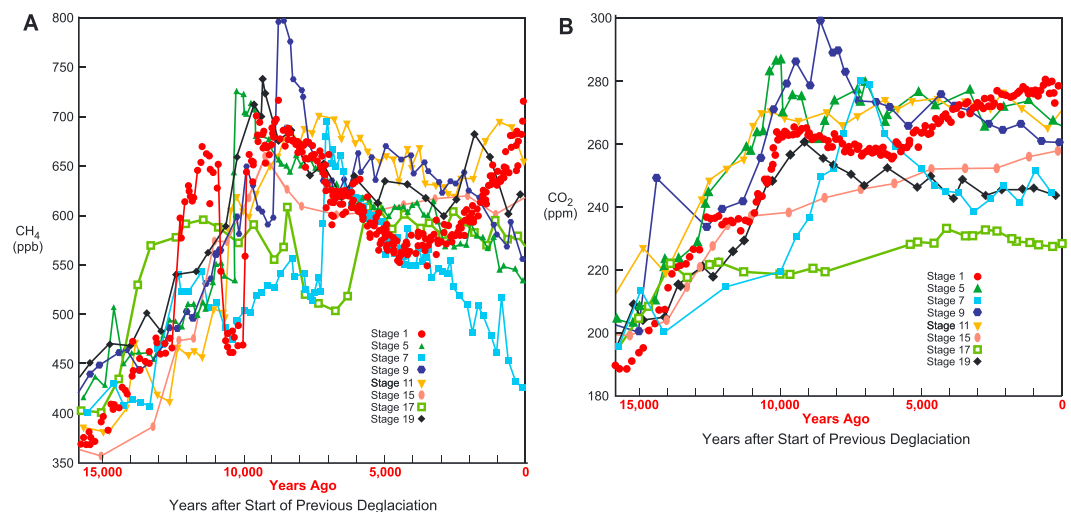
Figure A2. CH_4 and CO_2 trends that result from aligning all interglaciations on the beginning of the preceding deglaciations [*Ruddiman et al.*, 2011].

Table A4. CH_4 and CO_2 Trends Resulting From Aligning the Beginning of the Preceding Deglaciations[a]

Interglaciation	CH_4 Trend	CO_2 Trend
Stage 5	decrease	decrease[c]
Stage 7	decrease	decrease[c]
Stage 9	decrease	decrease
Stage 11[b]	decrease > increase[b]	NA[b]
Stage 15[b]	increase[b]	increase[b]
Stage 17[b]	decrease[b,c]	increase[b,c]
Stage 19	decrease	decrease[c]

[a]Natural explanations predict CH_4 increases (like the current interglaciation). Anthropogenic explanation predicts CH_4 decreases (unlike the current interglaciation). NA: no net overall trend.
[b]Entire interval falls on preceding deglaciation.
[c]Small-amplitude trend.

Aligning on obliquity (*tilt*). Changes in orbital obliquity at the 41,000 year cycle can also be used to align interglaciations. For the Holocene, the most recent maximum in tilt (as well as summer and annual insolation at high northern latitudes) occurred 10,000 years ago, just after the maximum in $\varepsilon\sin\omega$ Northern Hemisphere insolation 11,000 years ago (Table A6). For previous interglacial stages 5, 9, 15, and 19, the maxima in tilt and $e\sin\omega$ are closely aligned (as they are during the Holocene), but for stages 7, 11, and 17, they are offset by 7000 to 10,000 years.

For these obliquity-based alignments, the gas trends during previous interglacial intervals equivalent to those in the late Holocene are variable (Table A7). For CH_4, five of the seven previous interglaciations (stages 5, 9, 11, 15, and 19) show downward trends, while one (stage 17) has an initial CH_4 increase followed by a later decrease.

The CO_2 trends decrease for two interglaciations and increase for four others (Table A7). However, the equivalent late Holocene intervals determined for interglacial stages 7 and 15 in this alignment fall entirely on the prior deglaciation and do not qualify for this comparison. With these eliminated, two CO_2 trends show weak increases, while two show CO_2 decreases.

The stacked-average plot for methane (Figure A5) varies erratically during the interval aligned with the early Holocene and then drops during the time aligned with the late Holocene CH_4 decrease. The trends are similar with and without stages 7 and 15 included.

The stacked CO_2 trend that includes stages 7 and 15 shows a slow rise during the time equivalent to the late Holocene CO_2 increase. But with stages 7 and 15 omitted, the stacked average CO_2 trend is flat during that time.

The peak in the CH_4 stack between 6500 and 1500 equivalent years ago differs from the peaks in the other comparisons near 11,000–10,000 years ago. This difference occurs because the Holocene equivalent intervals
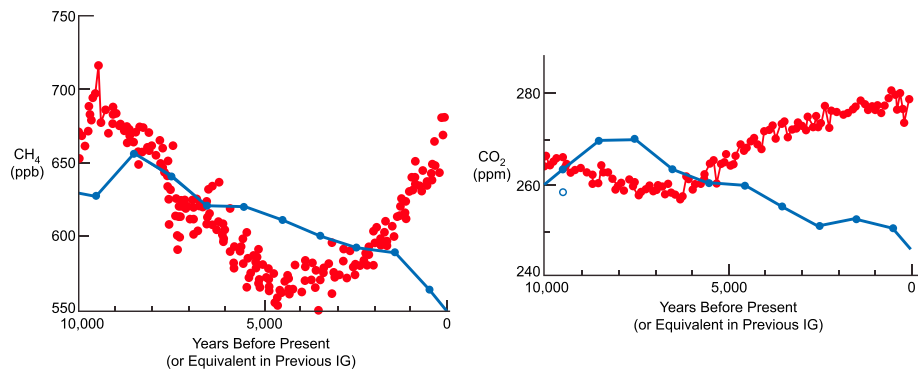
Figure A3. Stacked averages of CH_4 and CO_2 for previous interglaciations based on aligning the start of the previous deglaciations. Stages 11, 15, and 17 are omitted because the intervals supposedly aligned with the late Holocene fall entirely on the prior deglaciation.

Table A5. CH$_4$ and CO$_2$ Trends During Previous Interglaciations Resulting From Aligning the End of the Preceding Deglaciations[a]
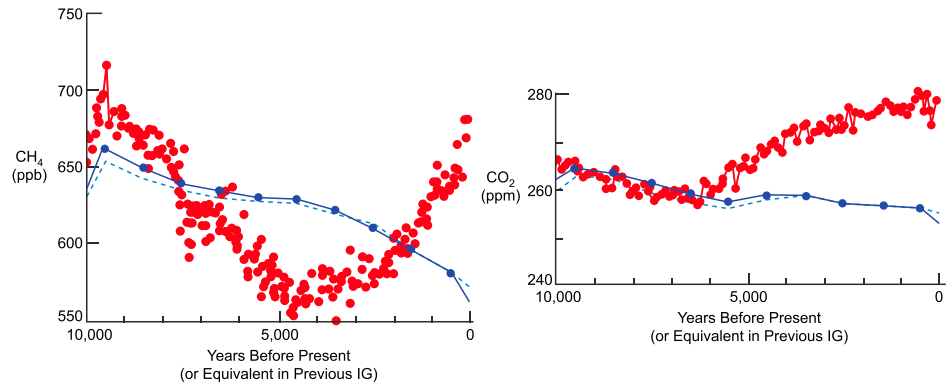
Interglaciation	CH$_4$ Trend	CO$_2$ Trend
Stage 5	decreasing	NA
Stage 7	decreasing	decreasing
Stage 9	NA	decreasing
Stage 11	decreasing[b]	NA
Stage 15[c]	decreasing[c]	increasing[c]
Stage 17	decreasing	increasing[b]
Stage 19	decreasing[d]	decreasing

[a]Natural explanations predict CH$_4$ increases (like the current interglaciation). Anthropogenic explanation predicts CH$_4$ decreases (unlike the current interglaciation). NA: no net overall trend.
[b]Small-amplitude trend.
[c]End of deglaciation not well defined; continues through interglacial.
[d]Short millennial-scale peak ignored.

Figure A4. Stacked averages of CH$_4$ and CO$_2$ for previous interglaciations based on aligning the end of the previous deglaciations. Solid blue trend shows average with stage 15 omitted; dashed trend shows trend with stage 15 included.

Table A6. Ages of Obliquity Maxima Used to Align the Holocene (Stage 1) With Previous Interglaciations, Compared to Ages of $e\sin\omega$ Minima (Northern Hemisphere Insolation Maxima)

| Interglacial Stage	Obliquity Maximum (years)	Prec Insol Maximum (years)
1	10,000	11,000
5	131,000	127,000
7	242,000	242,000
9	333,500	334,500
11	416,000	409,000
15	621,500	621,000
17	703,000	694,000
19	787,500	788,000

in stages 5, 11, and 17 for the obliquity-aligned time scale occur later than in the other time scales. This delayed timing pushes the early Holocene CH$_4$ peaks into the middle Holocene, and it also suppresses the early Holocene CO$_2$ peak and its decrease during the late Holocene.

The upward CO$_2$ trend in the obliquity comparison that includes all interglacial stages is the only evidence found here of a trend that agrees with natural explanations of the Holocene CO$_2$ increase. However, with the two invalid interglaciations removed, the CO$_2$ trend is flat and it no longer supports the natural explanations. In summary, the three additional comparisons summarized here favor the downward CO$_2$ and CH$_4$ trends predicted by the early anthropogenic hypothesis. None shows clear evidence of upward trends as predicted by natural explanations of the late Holocene [*Broecker et al.*, 1999; *Ridgwell et al.*, 2003].

Table A7. CH_4 and CO_2 Trends During Previous Interglaciations: Obliquity-Alignment Method[a]

Interglaciation	CH_4 Trend	CO_2 Trend
Stage 5	decrease	NA
Stage 7[b]	NA[b]	increase[b]
Stage 9	decrease	decrease
Stage 11	decrease[d]	increase[d]
Stage 15[b]	decrease[db]	increase[b]
Stage 17	increase > decrease	increase[d]
Stage 19	decrease[c]	decrease

[a]Natural explanations predict CH_4 and CO_2 increases (like the current interglaciation). Anthropogenic explanation predicts CH_4 and CO_2 decreases (unlike the current interglaciation). NA: no net trend.
[b]Entire interval falls on preceding deglaciation.
[c]Short millennial-scale peak ignored.
[d]Small-amplitude trend.
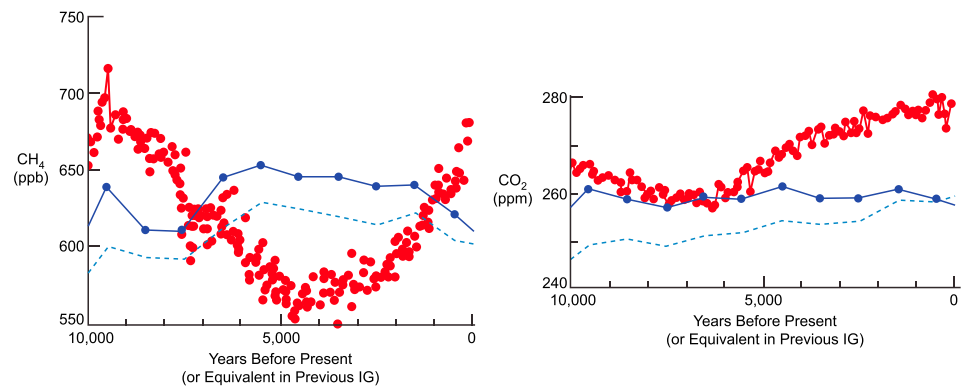
Figure A5. Stacked averages of CH_4 and CO_2 for previous interglaciations based on aligning obliquity maxima. Solid blue trend shows the average with stages 7 and 15 omitted; dashed trend shows trend with them included.

Appendix B: The Closest Insolation Analog to the Holocene

A perfect insolation analog for the Holocene would have obliquity and precession variations identical in both magnitude and relative timing. No such analog exists.

Several earlier studies recommended stage 11 as the best insolation analog, including *EPICA Community Members* [2004] and *Broecker and Stocker* [2006]. This choice was based on the fact that the $esin\omega$ signal for both interglaciations had very nearly the same amplitude (text Figure 5a), but it ignored the fact that the signals for obliquity, also an important source of orbital forcing, were out of alignment between the two interglaciations (text Figure 5b). Subsequent investigations have shown that stage 19 is the best insolation analog (text Figures 5a and 5b) during the 800,000 year time interval spanned by Dome C ice [*Tzedakis et al.*, 2012; *Berger and Yin*, 2012]. In addition, recent Ar/Ar dating [*Giaccio et al.*, 2015] confirms an age for interglacial stage 19 consistent with estimates in both the Dome C ice core record [*Parrenin et al.*, 2007] and the marine benthic oxygen isotopic stack [*Lisiecki and Raymo*, 2005].

The CO_2 signal during the earliest part of interglacial stage 19 agrees reasonably well with early stage 1, with a 262 ppm peak compared to the 268 ppm peak in the Holocene (text Figure 5c). But later the agreement ends, with the Holocene trend after 7000 years ago rising to an eventual preindustrial peak above 280 ppm, while the stage 19 concentration for the comparable interval falls to 245 ppm. The latter value is at the top of the 240–245 ppm range estimated for a current world free of all anthropogenic gas emissions [*Ruddiman*, 2003].

But the stage 19 greenhouse gas analog is not perfect. The stage 19 CH_4 trend remained at values higher than the presumably natural part of the Holocene CH_4 trend between 6000 and 3000 years ago and never fell below the 560 ppb level reached 5000 years ago. As a result, the stage 19 CH_4 signal is not a perfect analog for an anthropogenic-free late Holocene.
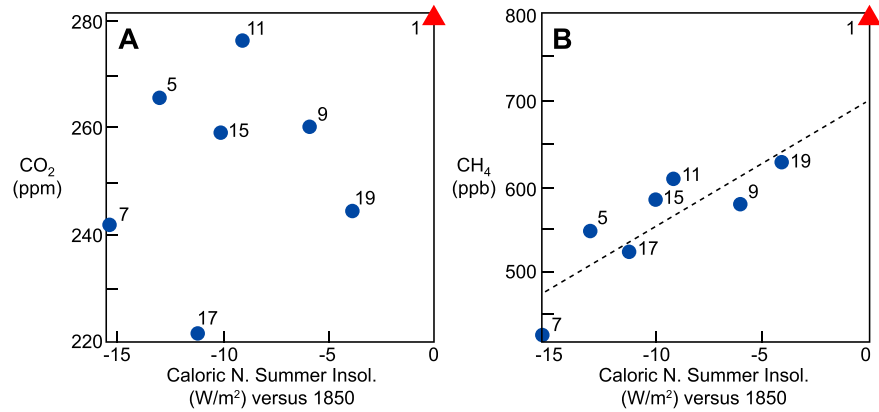
Figure B1. CO_2, CH_4, and summer half-year caloric insolation anomalies compared to Holocene (year 1850) values. Dashed line shows correlation of pre-Holocene values.

Another way to analyze natural CO_2 and CH_4 trends in previous interglaciations is to construct stacked averages of the previous trends [*Ruddiman et al.*, 2011]. The CH_4 and CO_2 stacks in text Figures 3a and 3b show downward trends consistent in direction with the early anthropogenic hypothesis, although the modern-day equivalent CO_2 level of 250 ppm in the stack is slightly higher than the 240–245 ppm value proposed in the early anthropogenic hypothesis, and the 545 ppb CH_4 is considerably higher than the proposed 450 ppb natural concentration.

Another way of comparing gas trends in previous interglaciations with those in the Holocene is to compare the latest preindustrial (1850) gas and insolation values against equivalent times during previous interglaciations. The plots in Figure B1 use caloric northern summer insolation values at 65°N from *Berger* [1978]. In both cases, the latest Holocene gas concentrations are higher than those in previous interglaciations, consistent in sense with the predictions of the early anthropogenic hypothesis. The pre-Holocene CO_2 values in Figure B1a are too scattered to suggest any clear relationship. The CH_4 levels in Figure B1b show a more suggestive correlation which appears to indicate a concentration of ~680 ppb for the insolation value during the late Holocene. As noted earlier, however, the natural CH_4 value 5000 years ago had already fallen well below that level to 560 ppb, so this method is not a valid way to estimate the anthropogenic-free late Holocene CH_4 concentration.
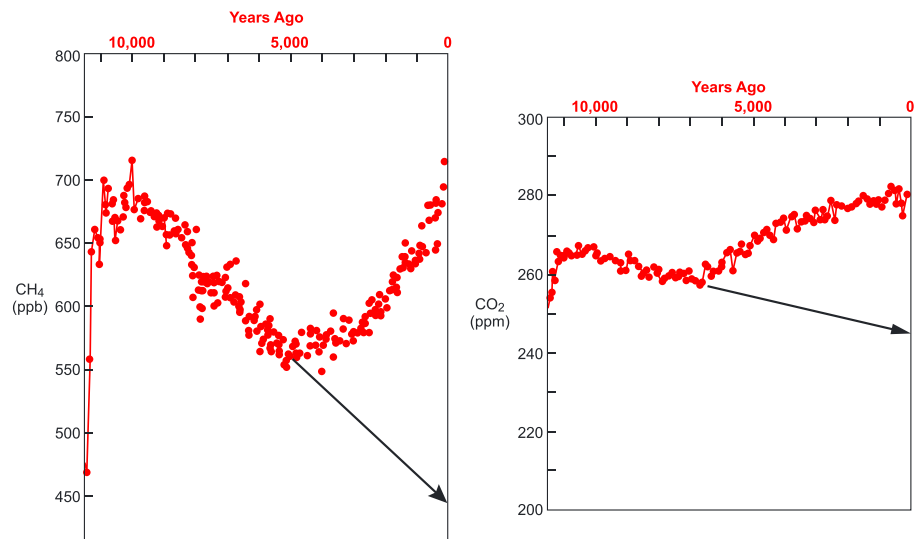
Figure B2. Linear projections (in black) of early Holocene CH_4 and CO_2 values forward to the industrial era (present day).

The scatter between the gas and insolation anomalies for the pre-Holocene interglaciations in Figure B1 could have several explanations. First, the prior histories of the relative timing and amplitude of the obliquity and precession forcing trends in the various interglaciations differ widely. As a result, climatic (and greenhouse gas) responses during the various late-deglacial and earliest interglacial climate pathways are also likely to have differed. In addition, dating errors in the EDC3 time scale (estimated at ±6000 years by *Parrenin et al.* [2007]) could mask part of the actual relationship.

Because of the problems noted above, *Ruddiman et al.* [2011] decided that the least controversial way to estimate the modern-day anthropogenic-free CO_2 and CH_4 concentrations would be to use the measured early Holocene CO_2 and CH_4 decreases (both assumed to have been natural) and project them forward to the present day, while avoiding the short-lived overshoot-like gas peaks that occurred early in some interglaciations. For the seven pre-Holocene interglacial examples, the rate of gas changes from early to late in the interglaciations decreased in some cases, increased in others, and remained about the same in still others (text Figures 2a and 2b). The average rate of change is approximately constant.

Based on this observation, *Ruddiman et al.* [2011] linearly projected the decreasing CO_2 and CH_4 trends during the early Holocene forward to the modern day (Figure B2). This method yielded anthropogenic-free industrial era (modern-day) estimates of 245 ppm for CO_2 and 445 ppb for CH_4, close to the values proposed in the original early anthropogenic hypothesis (250 ppm and 450 ppb). Despite its obvious uncertainties, this approach has two advantages: (1) it uses actual Holocene data as the starting point and (2) it makes projections consistent with average behavior during equivalent times in previous interglaciations.

References

Arbuckle, B. S. (2014), Pace and progress in the emergence of animal husbandry in Neolithic Southwest Asia, *Bioarchaeol Near East*, 8, 53–81.

Bereiter, B., S. Eggleston, J. Schmitt, C. Nehrbass-Ahles, T. F. Stocker, H. Fischer, S. Kipfstuhl, and J. Chappellaz (2015), Revision of the EPICA Dome C CO_2 record from 800 to 600 kyr before present, *Geophys. Res. Lett.*, 42, 542–549, doi:10.1002/2014GL061957.

Berger, A. (1978), Long-term variations in caloric insolation resulting from the Earth's orbital elements, *Quat. Res.*, 9, 139–167.

Berger, A. L., and Q. Yin (2012), Modeling the past and future interglacials in response to astronomical and greenhouse gas forcing, in *The Future of the Worlds Climate*, edited by A. Henderson-Sellers and K. McGuffie, pp. 437–462, Elsevier, Amsterdam.

Boivin, N., and D. Q. Fuller (2009), Shell middens, ships and seeds: Exploring coastal subsidence, maritime trade, and the dispersal of domesticates in and around the ancient Arabian Peninsula, *J. World Prehistory*, 22, 113–180.

Boserup, E. (1981), *Population and Technological Change: A Study of Long Term Trends*, Univ. Chicago Press, Chicago.

Bradley, R. S. (1999), *Paleoclimatology: Reconstructing Climates of the Quaternary*, Int. Geophys. Ser., vol. 64, Harcourt Acad. Press, San Diego, Calif.

Broecker, W. S., and T. L. Stocker (2006), The Holocene CO_2 rise: Anthropogenic or natural?, *Eos Trans. AGU*, 87, 27, doi:10.1029/2006EO030002.

Broecker, W. S., E. Clark, D. McCorckle, T.-H. Peng, I. Hajdas, and G. Bonani (1999), Evidence for a reduction in the carbonate ion content of the deep sea during the course of the Holocene, *Paleoceanography*, 14, 744–752.

Buck, J. L. (1937), *Land Utilization in China*, Commercial Press, Changhai.

Chao, K. (1986), *Man and Land in Chinese History: An Economic Analysis*, Stanford Univ. Press, Stanford.

Colledge, S., J. Conolly, K. Dobney, K. Manning, and S. Shennan (2013), *The Origins and Spread of Domestic Animals in Southwest Asia and Europe*, Left Coast Press, Walnut Creek, Calif.

Conolly, J., S. Colledge, K. Dobney, J.-D. Vigne, J. Peters, B. Stopp, K. Manning, and S. Shennan (2011), Meta-analysis of zooarchaeological data from SW Asia and SE Europe provides insight into the origins and spread of animal husbandry, *J. Archaeol. Sci.*, 38, 538–545.

Dodson, J., X. Li, N. Sun, P. Atahan, X. Zhou, H. Liu, K. Zhao, S. Hu, and Z. Yang (2014), Use of coal in the Bronze Age in China, *Holocene*, 24, 525–530.

Ellis, E. C., and S. M. Wang (1997), Sustainable traditional agriculture in the Tai Lake region of China, *Afr. Ecosyst. Environ.*, 61, 177–193.

Ellis, E. C., J. O. Kaplan, D. Q. Fuller, S. Vavrus, K. Klein Goldwijk, and P. Verburg (2013), Used planet: A global history, *Proc. Natl. Acad. Sci. U.S.A.*, 110, 7978–7985.

Elsig, J., J. Schmitt, D. Leuenberger, R. Schneider, M. Eyer, M. Leuenberger, F. Joos, H. Fischer, and T. Stocker (2009), Stable isotope constraints on Holocene carbon cycle changes from an Antarctic ice core, *Nature*, 461, 507–510.

EPICA Community Members (2004), Eight glacial cycles from an Antarctic ice core, *Nature*, 429, 623–628.

Fuller, D. Q. (2011), Finding plant domestication in the Indian subcontinent, *Curr. Anthropol.*, 52, 5347–5362.

Fuller, D. Q., J. van Etten, K. Manning, E. Kingwell-Banham, A. Weisskopf, L. Qin, Y. I. Sato, and R. Hijmans (2011), The contribution of rice agriculture and livestock to prehistoric methane levels: An archeological assessment, *Holocene*, 21, 743–759.

Fuller, D. Q., T. Denham, M. Arroyo-Kalin, L. Lucas, C. J. Stevens, L. Qin, R. G. Allaby, and M. Purugganan (2014), Convergent evolution and parallelism in plant domestication revealed by an expanding archaeological record, *Proc. Natl. Acad. Sci. U.S.A.*, 111, 6147–6152.

Fyfe, R. M., J. Woodbridge, and N. Roberts (2015), From forest to farmland: pollen-inferred land cover changes across Europe using the pseudobiomization approach, *Global Change Biol.*, 20, 1197–1212.

Ganopolski, A., and V. Brovkin (2015), The last four glacial CO_2 cycles simulated with the Climber-2 model, *Nova Acta Leopold*,, 121, 75–79.

Giaccio, B., et al. (2015), Duration and dynamics of the best orbital analogue to the present interglacial, *Geology*, doi:10.1130/G36677.1.

Gignoux, C. R., B. M. Henn, and J. L. Mountain (2011), Rapid global demographic expansions after the origins of agriculture, *Proc. Natl. Acad. Sci. U.S.A.*, 108, 6044–6049.

Gorham, E. (1991), Northern peatlands: Role in the carbon cycle and probable responses to climatic warming, *Ecol. Appl.*, 1, 182–195.

Hays, J. D., J. I. Imbrie, and N. J. Shackleton (1976), Variations in the Earth's orbit: Pacemaker of the ice ages, *Science*, 194, 1121–1132.

He, F., S. J. Vavrus, J. E. Kutzbach, W. F. Ruddiman, and P. C. Tzedakis (2013), Glacial inception during the late Holocene without carbon emissions from early agriculture: Lessons from the stage-19 glacial inception, in AGU Fall Meeting Abstracts 1, 1000.

Hoffman, T., et al. (2013), Humans and the missing C-sink: Erosion and burial of soil carbon through time, *Earth Surf. Dyn. Discuss.*, *1*, 1–20.

Horel, J., and J. Geisler (1996), *Global Environmental Change: An Atmospheric Perspective*, John Wiley, New York.

Imbrie, J., et al. (1984), The orbital theory of Pleistocene climate: Support from a revised chronology of the marine $\delta^{18}O$ record, in *Milankovitch and Climate*, edited by A. Berger et al., pp. 269–305, Reidel, Dordrecht.

Imbrie, J., et al. (1992), On the structure and origin of major glaciation cycles: I. Linear responses to Milankovitch forcing, *Paleoceanography*, *7*, 701–738.

Joos, F., S. Gerber, I. C. Prentice, B. L. Otto-Bleisner, and P. Valdes (2004), Transient simulations of Holocene atmospheric carbon dioxide and terrestrial carbon since the last glacial maximum, *Global Biogeochem. Cycles*, *18*, GB2002, doi:10.1029/2003GB002156.

Jouzel, J., et al. (2003), Magnitude of isotope/temperature scaling for interpretation of central Antarctic ice cores, *J. Geophys. Res.*, *108*(D12), 4361, doi:10.1029/2002JD002677.

Kaplan, J. O., K. M. Krumhardt, and N. Zimmerman (2009), The prehistorical and preindustrial deforestation of Europe, *Quat. Sci. Rev.*, *28*, 3016–3034.

Kaplan, J. O., K. M. Krumhardt, E. C. Ellis, W. F. Ruddiman, C. Lemmen, and K. Goldewijk (2011), Holocene carbon emissions as a result of anthropogenic land cover change, *Holocene*, *21*, 775–792.

Kingwell-Banham, E., and D. Q. Fuller (2012), Shifting cultivators in South Asia: Expansion, marginalization and specialization over the long term, *Quat. Int.*, *249*, 84–95.

Kleinen, T., V. Brovkin, and R. J. Schuldt (2012), A dynamic model of wetland extent and peat accumulation: Results for the Holocene, *Biogeosciences*, *9*, 235–248, doi:10.5194/bg-9-235-2012.

Kleinen, T., V. Brovkin, and G. Munhoven (2015), Carbon cycle dynamics during recent interglacials, *Clim. Past Discuss.*, *11*, 1945–1983.

Klinger, L. F., J. A. Taylor, and L. G. Franzen (1996), The potential role of peatland dynamics in ice-age initiation, *Quat. Res.*, *45*, 89–92.

Kutzbach, J. E., S. K. Vavrus, W. F. Ruddiman, and G. Phillipon-Berthier (2011), Comparisons of atmosphere–ocean simulations of greenhouse gas-induced climate change for preindustrial and hypothetical "no-anthropogenic" radiative forcing, relative to the present day, *Holocene*, *21*, 853–864.

Kutzbach, J. E., F. He, S. J. Vavrus, and W. F. Ruddiman (2013), The dependence of equilibrium climate sensitivity on climate state: Applications to studies of climate colder than present, *Geophys. Res. Lett.*, *40*, 3721–3726, doi:10.1002/grl.50724.

Larson, G., et al. (2014), Current perspectives and the future of domestication studies, *Proc. Natl. Acad. Sci. U.S.A.*, *111*, 6139–6146.

Lemmen, C. (2010), World distribution of land cover changes during Pre- and Protohistoric Times and estimation of induced carbon releases, *Géomorphol. Reli. Process. Environ.*, *4*, 303–312.

Li, X., J. Dodson, J. Zhou, and X. Zhou (2009), Increases of population and expansion of rice agriculture in Asia, and anthropogenic methane emissions since 5000 BP, *Quat. Int.*, *202*, 41–50.

Lisiecki, L. E., and M. E. Raymo (2005), A Pliocene-Pleistocene stack of 57 globally distributed benthic $\delta^{18}O$ records, *Paleoceanography*, *20*, PA1003, doi:10.1029/2004PA001071.

Luthi, D., et al. (2008), High-resolution carbon dioxide concentration record 650,000-800,000 years before present, *Nature*, *453*, 379–382.

Marlon, J. R., P. J. Bartlein, A. L. Daniau, S. P. Harrison, S. Y. Maezumi, M. J. Power, W. Tinner, and B. Vanniere (2013), Global biomass burning: A synthesis and review of Holocene paleofire records and their controls, *Quat. Sci. Rev.*, *65*, 5–25.

Masson, V., et al. (2000), Holocene climate variability in Antarctica based on 11 ice-core isotopic records, *Quat. Res.*, *54*, 348–358.

Mather, A. S., and C. L. Needle (2000), The relationships of population and forest trends, *Geogr. J.*, *166*, 2–13.

Milankovitch, M. (1941), *Kanon der Erdbestrahlung und seine Andwendung auf das Eiszeitenproblem*, vol. 133, 633 pp., Royal Serbian Academy Special Publication, Belgrade [English translation published in 1969 by Israel Program for Scientific Translations, U.S. Dept. Comm.]

Monnin, E., A. Indermühle1, A. Dällenbach, J. Flückiger, B. Stauffer, T. F. Stocker, D. Raynaud, and J.-M. Barnola (2001), Atmospheric CO_2 concentrations over the last glacial termination, *Science*, *291*, 112–114.

Parrenin, F., et al. (2007), The EDC3 chronology for the EPICA Dome C ice core, *Clim. Past*, *3*, 485–497.

Petit, J. R., et al. (1999), Climate and atmospheric history of the past 420,000 years from the Vostok ice core, Antarctica, *Nature*, *399*, 429–436.

Pongratz, J., C. Reick, T. Raddatz, and M. A. Claussen (2008), A reconstruction of global agricultural areas and land cover for the last millennium, *Global Biogeochem. Cycles*, *22*, GB3018, doi:10.1029/2008GLO36394.

Raymo, M., W. F. Ruddiman, J. Backman, B. M. Clement, and D. M. Martinson (1989), Late Pliocene variation in northern hemisphere ice sheets and North Atlantic Deep Water circulation, *Paleoceanography*, *4*, 413–446.

Ren, G. (2007), Changes in forest cover in China during the Holocene, *Veg. Hist. Archaeobot.*, *16*, 119–126.

Ridgwell, A. J., M. A. Watson, M. A. Maslin, and J. O. Kaplan (2003), Implications of coral reef buildup for the controls of atmospheric CO_2 since the Last Glacial Maximum, *Paleoceanography*, *18*, 1083, doi:10.1029/2003PA000893.

Ruddiman, W. F. (2003), The anthropogenic greenhouse era began thousands of years ago, *Clim. Change*, *61*, 261–293.

Ruddiman, W. F. (2007), The early anthropogenic hypothesis: Challenges and responses, *Rev. Geophys.*, *45*, RG4001, doi:10.1029/2006RG000207.

Ruddiman, W. F. (2008), The challenge of modeling interglacial CO_2 and CH_4 trends, *Quat. Sci. Rev.*, *27*, 445–448.

Ruddiman, W. F., J. E. Kutzbach, and S. J. Vavrus (2011), Can natural or anthropogenic explanations of late-Holocene CO_2 and CH_4 increases be falsified?, *Holocene*, *21*, 865–879.

Schneider, R., J. Schmitt, P. Kohler, F. Joos, and H. Fischer (2013), Reconstruction of atmospheric carbon dioxide and its carbon isotopic composition from the penultimate glacial maximum to the last glacial inception, *Clim. Past*, *9*, 2507–2523.

Schneider van Deimling, T., M. Meinshausen, A. Leverman, V. Huber, K. Frieler, D. M. Lawrence, and V. Brovkin (2012), Estimating the near-surface permafrost-carbon feedback on global warming, *Biogeosciences*, *9*, 649–665, doi:10.5194/bg-9-649-2012.

Selzer, G., D. Rodbell, and S. J. Burns (2000), Isotopic evidence for late glacial and Holocene hydrologic changes in tropical and South America, *Geology*, *28*, 35–38.

Shackleton, N. J., et al. (1984), Oxygen isotope calibration of the onset of ice rafting and history of glaciation in the North Atlantic region, *Nature*, *307*, 620–623.

Simmons, C. T., L. A. Mysak, and H. D. Mathews (2013), Investigation of the natural carbon cycle since 6000 B.C. using an intermediate complexity model: The role of Southern Ocean ventilation and marine ice shelves, *Atmos. Ocean*, *51*, 187–212.

Singarayer, J. S., P. J. Valdes, P. Friedlingstein, S. Nelson, and J. D. Beerling (2011), Late Holocene methane rise caused by orbitally controlled increase in tropical sources, *Nature*, *470*, 82–85.

Spahni, R., F. Joos, B. D. Stocker, M. Steinacher, and Z. Yu (2013), Transient simulations of the carbon and nitrogen dynamics in northern peatlands: From the Last Glacial Maximum to the 21st century, *Clim. Past*, *9*, 1287–1308.

Stern, J. V., and L. E. Lisiecki (2015), Termination 1 timing in radiocarbon-dated regional benthic $\delta^{18}O$ stacks, *Paleoceanography*, *29*, 1127–1142, doi:10.1002/2014PA002700.

Stocker, B. D., K. Strassmann, and F. Joos (2011), Sensitivity of Holocene atmospheric CO_2 and the modern carbon budget to early human land use: Analyses with a process-base model, *Biogeosciences*, *8*, 69–88.

Strassmann, K. M., F. Joos, and H. Fischer (2008), Simulating effects of land use changes on carbon fluxes: Past contributions to atmospheric CO_2 increases and future commitments due to losses of terrestrial sink capacity, *Tellus B*, *60*, 583–603.

Timpson, A., S. Colledgea, E. Cremaa, K. Edinborougha, T. Kerigc, K. Manninga, M. G. Thomasb, and S. Shennana (2014), Reconstructing regional population fluctuations in the European Neolithic using radiocarbon dates: A new case-study using an improved method, *J. Archaeol. Sci.*, *52*, 549–557.

Tzedakis, P. C. (2010), The MIS 11–MIS 1 analogy, southern European vegetation, atmospheric methane and the "early anthropogenic hypothesis", *Clim. Past*, *6*, 131–144.

Tzedakis, P. C., J. E. T. Channell, D. A. Hodell, H. F. Kleiven, and L. K. Skinner (2012), Determining the length of the current interglacial, *Nat. Geosci.*, *5*, 138–141.

Vavrus, S. J., W. F. Ruddiman, and J. E. Kutzbach (2008), Climate model tests of the anthropogenic influence on greenhouse-induced climate change: The role of early human agriculture, industrialization, and vegetation feedbacks, *Quat. Sci. Rev.*, *27*, 1410–1425, doi:10.1016/j.quascirev.2008.04.01.

Vavrus, S. J., G. Phillipon-Berthier, J. E. Kutzbach, and W. F. Ruddiman (2011), The role of GCM resolution in simulating glacial inception, *Holocene*, *21*, 819–830.

Wagner, M., P. Tarasov, D. Hosner, A. Fleck, R. Ehrich, X. Chen, and C. Liepe (2013), Mapping of the spatial and temporal distribution of archaeological sites of northern China during the Neolithic and Bronze Age, *Quat. Int.*, *290*, 344–357.

Wirtz, K. W., and C. Lemmen (2003), A global dynamic model for the Neolithic transition, *Clim. Change*, *59*, 333–367.

Woodbrige, J., R. M. Fyfe, N. Roberts, S. Downey, K. Edinborough, and S. Shennan (2014), The impact of the Neolithic agricultural transition in Britain: A comparison of pollen-based land-cover and archaeological ^{14}C-date-inferred population change, *J. Archaeol. Sci.*, *51*, 216–224.

Yu, Z. (2011), Holocene carbon flux histories of the world's peatlands: Global carbon-cycle implications, *Holocene*, *21*, 761–774.

Zennaro, P., N. Kehrwald, J. Marlon, W. Ruddiman, T. Brucher, C. Agostinelli, D. Dahl-Jensen, R. Zangrando, A. Gambarro, and C. Barbante (2015), Europe on fire three thousand years ago: Arson or climate?, *Geophys. Res. Lett.*, *42*, 5023–5033, doi:10.1002/2015GL064259.

Zimov, N. S., S. A. Zimov, A. E. Zimova, G. M. Zimova, V. I. Chuprynin, and F. S. Chapin (2009), Carbon storage in permafrost and soils of the mammoth tundra-steppe biome, *Geophys. Res. Lett.*, *3*, LO2502, doi:10.1029/2008GL036332.

Zohary, D., M. Hopf, and E. Weiss (2012), *Domestication of Plants in the Old World*, 4th ed., Oxford Univ. Press, Oxford.